Oxide route for production of Cu_2ZnSnS_4 solar cells by pulsed laser deposition

Gansukh, Mungunshagai; Mariño, Simón López; Espindola Rodriguez, Moises; Engberg, Sara Lena Josefin; Martinho, Filipe Mesquita Alves; Hajijafarassar, Alireza; Schjødt, Niels Christian; Stamate, Eugen; Hansen, Ole; Schou, Jørgen

Total number of authors:
11

Published in:
Solar Energy Materials and Solar Cells

Link to article, DOI:
10.1016/j.solmat.2020.110605

Publication date:
2020

Document Version
Peer reviewed version

Elsevier Editorial System(tm) for Solar Energy Materials and Solar Cells
Manuscript Draft

Manuscript Number: SOLMAT-D-20-00423R2

Title: Oxide route for production of Cu2ZnSnS4 solar cells by Pulsed Laser Deposition

Article Type: Full Length Article

Keywords: Cu2ZnSnS4 solar cells; Sn loss; Pulsed Laser Deposition; Oxide precursors; Oxy-sulfide precursors; Sulfide precursors

Corresponding Author: Dr. Stela Canulescu,

Corresponding Author's Institution: Technical University of Denmark

First Author: Mungunshagai Gansukh

Order of Authors: Mungunshagai Gansukh; Simón López Mariño; Moises Espindola Rodriguez; Sara Lena Josefin Engberg; Filipe Mesquita Alves Martinho; Alireza Hajijafarassar; Niels Christian Schjødt; Eugen Stamate; Ole Hansen; Jørgen Schou; Stela Canulescu

Abstract: In this work, we have investigated Cu2ZnSnS4 (CZTS) solar cells made from oxide, oxy-sulfide and sulfide precursors produced by pulsed laser deposition (PLD). Although sulfide precursors are widely used to fabricate CZTS solar cells, Sn loss is commonly observed due to the high volatility of SnxSy species during high temperature sulfurization. This can lead to a non-ideal absorber composition and a high density of detrimental Sn-related defects that severely affect the performance of the device. By using oxide precursors, we have shown that the Sn loss can be significantly reduced due to the higher thermal stability of SnxOy species when compared to their sulfide counterparts. However, the reaction mechanism for the oxide route results in rough CZTS films. We hypothesize that the SO2 gas that forms during the conversion from oxide to sulfide is trapped in the film during sulfurization, and can lead to grains with hollow cavities and thus increase the surface roughness. Therefore, we have developed an annealing route for the oxide precursors at lower annealing pressures, which leads to improved film morphology and device performance. As a result, we report a power conversion efficiency of 5.4% for solar cells made from oxide precursors. This is the highest value reported for a CZTS absorber produced by PLD.

Research Data Related to this Submission

Title: Oxide route for production of Cu2ZnSnS4 solar cells by Pulsed Laser Deposition
Repository: Mendeley Data
https://data.mendeley.com/drafts/

Highlights

- CZTS was prepared by sulfurization of oxide, oxy-sulfide and sulfide precursors;
- The effect of annealing conditions on the performance of CZTS was investigated;
- Annealing of the oxides at low pressure is beneficial as it reduces roughness;
- SnOxSy layer forms at the back contact after sulfurization at high pressure;
- CZTS cells fabricated from oxides show the highest efficiency made by PLD (5.4%);

Oxide route for production of Cu_2ZnSnS_4 solar cells by Pulsed Laser Deposition

Mungunshagai Gansukh[1], Simón López Mariño[2], Moises Espindola Rodriguez[3], Sara Lena Josefin Engberg[1], Filipe Mesquita Alves Martinho[1], Alireza Hajijafarassar[2], Niels Christian Schjødt[4], Eugen Stamate[2], Ole Hansen[2], Jørgen Schou[1] and Stela Canulescu[1]*

[1]Department of Photonics Engineering, Technical University of Denmark, DK-4000 Roskilde, Denmark

[2]DTU Nanolab, National Center for Nano Fabrication and Characterization, Technical University of Denmark, DK-2800 Kgs. Lyngby, Denmark

[3]Department of Energy Conversion and Storage, Technical University of Denmark, DK-2800 Kgs. Lyngby, Denmark

[4]Haldor Topsøe A/S, Haldor Topsøes Allé 1, DK-2800 Kgs. Lyngby, Denmark

[*]Corresponding author Stela Canulescu, email: stec@fotonik.dtu.dk

Keywords

Cu_2ZnSnS_4 solar cells; Sn loss; Pulsed Laser Deposition; Oxide precursors; Oxy-sulfide precursors; Sulfide precursors

Abstract

In this work, we have investigated Cu_2ZnSnS_4 (CZTS) solar cells made from oxide, oxy-sulfide and sulfide precursors produced by pulsed laser deposition (PLD). Although sulfide precursors are widely used to fabricate CZTS solar cells, Sn loss is commonly observed due to the high volatility of Sn_xS_y species during high temperature sulfurization. This can lead to a non-ideal absorber composition and a high density of detrimental Sn-related defects that severely affect the performance of the device. By using oxide precursors, we have shown that the Sn loss can be significantly reduced due to the higher thermal stability of Sn_xO_y species when compared to their sulfide counterparts. However, the reaction mechanism for the oxide route results in rough CZTS films. We hypothesize that the SO_2 gas that forms during the conversion from oxide to sulfide is trapped in the film during sulfurization, and can lead to grains with hollow cavities and thus increase the surface roughness. Therefore, we have developed an annealing route for the oxide precursors at lower annealing pressures, which leads to improved film morphology and device performance. As a result, we report a power conversion efficiency of 5.4% for solar cells made from oxide precursors. This is the highest value reported for a CZTS absorber produced by PLD.

1. Introduction

Cu_2ZnSnS_4 (CZTS) is a promising p-type solar cell absorber material that has a nearly ideal bandgap for single junction solar cells (~1.5 eV) and a high absorption coefficient[1–4]. It consists of earth abundant and non-toxic elements. The CZTS solar cells have reached an efficiency of 11%[5] and the $Cu_2ZnSn(S,Se)_4$ (CZTSSe) solar cells an efficiency of 12.6%[6]. The challenges associated with the moderate efficiency of the kesterite devices include low

open circuit voltage (V_{OC}), which can stems from a large density of Sn- and S-related deep level defects[7–9].

Most of the CZTS absorbers are made from metallic or sulfide precursors. This is a logical choice as there are no foreign elements included in these compound, such as oxygen, and the conversion into a sulfide material is easy[10]. Nevertheless, due to the volatile nature of Sn_xS_y species, the final composition of the film after conversion will likely have less Sn compared to the initial composition[11,12]. It has been shown that adding a small amount of Sn powder during annealing process improves the overall performance of the solar cells[13]. Alternatively, one can employ oxide compounds as a precursor for the fabrication of CZTS devices. In this case, oxides are advantageous over their sulfide counterparts due to their high temperature stability. In addition, they can be used for an additive-free solution processing route that can be processed on large scale[10]. In a solution-processing route, solvents and additives typically contain carbon and halogens. Removing these species can be difficult, and their incomplete removal can hamper the device performance. When using oxide precursors, it is possible to use pre-annealing in air to effectively burn out and thus remove remaining organic species and halogens. Combustion occurs when organic material is heated in air, and it will leave the films with less carbon residues[14,15]. Moreover, pre-annealing of oxides in air could be a low-cost and relatively environmental-friendly process[10,15]. This approach may open new opportunities for the mass production of high quality CZTS films made from a low-cost solution-processing path.

However, there are only a few cases in which CZTS made from oxide precursors have been studied. Washio et al. have reported on a 6% efficient CZTS solar cell by an open atmosphere type chemical vapor deposition method, which is the highest efficiency of a cell made from oxide precursors[16]. Jin et al. have reported on CZTS solar cells made by pulsed laser deposition (PLD) from oxide precursors, and achieved an efficiency of 4.94%[17]. They also

studied the formation mechanism of CZTS from an oxide powder and observed that SO_2 gas is formed during sulfurization[14]. First principles simulation suggest that the $Cu_2ZnSnS_xO_{4-x}$ (CZTSO) alloy might exist[18], but to the best of our knowledge, this has not been validated yet. While the possibility of tuning the band gap by varying the S/O ratio may enable the use of CZTSO in tandem solar cell configurations[19,20], oxygen alloying of CZTS remains to be demonstrated. PLD is an emerging technique for the synthesis of chalcogenide materials and it allows deposition of compounds with complex stoichiometry, while providing a fine control over the deposition rate. PLD relies on nearly stoichiometric transfer of the ablated material from a target to a substrate on a typical time scale of microseconds after the laser pulse[21]. The plasma plume features species with kinetic energies of tens of eV[22], which upon landing on the substrate leads to the formation of a uniform film ("the precursor film"). It is worth noting that pulsed laser deposition can lead to a pronounced decrease in the optical transmission of the laser window in the PLD system, resulting in a significant reduction of the fluence[23]. In this study, we have investigated the formation mechanism of CZTS from oxide precursors produced by PLD. We find that CZTS grains with hollow cavities, a kind of bubble-like structure, were formed when oxide precursors were used. The burst of these bubbles results in a non-compact film which affects device performance. We hypothesize that the release of SO_2 during the sulfurization process is the main reason for the non-compact films, and that it potentially could be controlled by changing the annealing pressure. By studying the influence of the N_2 pressure on the sulfurization process, we show that a low pressure results in a more compact film and a complete sulfurization of the oxides. Finally, we compare solar cells made from oxide, oxy-sulfide and sulfide precursors.

2. Experimental

2.1 Materials and device fabrication

Oxide, oxy-sulfide and sulfide precursors were grown by PLD, using a procedure described in previous studies[23,24]. The oxide (from Haldor Topsøe), oxy-sulfide (from Haldor Topsøe), and sulfide targets (from Testbourne Ltd) made of oxide and sulfide binary compounds with metal ratios of Cu/(Zn+Sn)~0.5 and Zn/Sn~1.1 and O/(O+S) ratios of 1, 0.3 and 0, respectively, were used. The targets were ablated by focusing a laser beam from an excimer laser (248 nm KrF, 20 ns FWHM and 15 Hz repetition rate) onto a spot area of 1.7 mm^2 at an angle of incidence of 45°. The average fluence was 2 J/cm^2. To avoid the previously mentioned decrease in optical transmission of the window and maintain a relatively constant fluence during deposition, an intelligent window (from PVD products) consisting of a rotating UV-graded silica disc in vacuum was used. The disc acts as a sacrificial window between the laser window and the plasma plume, which rotates during deposition exposing always a new optical surface. The typical deposition rates for oxide, oxy-sulfide and sulfide were 4.1, 7.3 and 8.7 nm/min, respectively, and the time for a deposition varied from 2 to 4 hours (at a laser frequency of 15 Hz). This suggests that the ablation yield of sulfides is much higher than that of oxides, presumably due to their highly volatile components. The precursor films were deposited in vacuum, with a base pressure below 10^{-6} mbar, on 2.5 × 2.5 cm^2 Mo-coated soda lime glass substrates (from the Center for Solar Energy and Hydrogen Research Baden-Wuerttemberg, ZSW). All films were grown at room temperature to minimize sulfur loss for the targets containing sulfur. The precursor films were cut into 1.25 × 1.25 cm^2 and placed in a graphite box with 120 mg S (99.998%, Sigma-Aldrich) and 5 mg Sn powder (≥99%, Sigma-Aldrich) and loaded into a tube furnace evacuated to a base pressure below 10^{-2} mbar. The precursors were then subjected to a two-step annealing procedure in nitrogen atmosphere: first, the samples were heated to 200 °C for 30 min under a flow of 1.5 mbar N_2, followed by heating to different temperatures of 540 °C, 560 °C and 580 °C for 30 min. For the morphological study for the oxide precursors, we have employed temperatures of 540°C and 560°C (Table 1) and

the rest of the samples, including oxide precursors for solar cells, were annealed at 580 °C. The nitrogen pressure in the high temperature annealing step was varied from 50, 250, 500 to 1000 mbar for comparing the oxide, oxy-sulfide and sulfide routes. The temperatures and nitrogen pressures in the second step of the annealing are listed in Table 2. Additional samples for each precursor were annealed at a pressure of 250 mbar without intentionally added Sn powder. To enable Raman measurements of CZTS from the backside, an additional oxide precursor film was deposited on sapphire substrate and annealed at 250 mbar, 580 °C for 30 min. The final thickness of the annealed CZTS layer is around 1 µm. After the annealing, the absorbers were etched in a $(NH_4)_2S$ solution[25] at room temperature for 5 min. Chemical bath deposition was used to produce a 65 nm CdS buffer layer. Finally, full solar cells were finished by depositing a 50 nm i-ZnO layer and 350 nm Al-doped ZnO layer as window layers by sputtering using a procedure described elsewhere[26]. All samples were post annealed at 250 °C for 1 min and cooled with the rate of 1 °C per min in N_2 atmosphere.

2.1 Characterization methods

Raman and photoluminescence (PL) measurements were done on finished solar cells using a Renishaw inVia Reflex confocal Raman microscope equipped with two excitations sources: a diode-pumped solid-state laser at 532 nm and a diode laser at 785 nm. The laser beam was focused onto the sample with a VIS-NIR 50× objective (NA 0.75). The scattered light was collected by the same objective lens and dispersed using a Renishaw inVia Reflex Spectrometer. Either a grating with 1800 grooves/mm or 2400 grooves/mm was used. X-ray diffraction (XRD) patterns were obtained in Bragg-Brentano configuration on a Bruker D8 diffractometer. Scanning electron microscopy (SEM) images were obtained by a Merlin field emission electron microscope from Carl Zeiss at 5 kV acceleration voltage with a HE-SE2 detector. Energy dispersive x-ray spectroscopy (EDX) measurements were done by TM3000 tabletop microscope from Hitachi at 15 kV electron acceleration voltage in order to measure the

elemental composition of the precursors, absorbers and PLD targets. External quantum efficiency (EQE) measurements were performed in a QEXL system from PV measurements on finished cells. Current density-voltage (JV) measurements were done with a Newport Sol2A Class ABA steady state solar simulator under standard test conditions, calibrated with a Si reference cell.

Table 1. Annealing parameters used for the oxide to sulfide conversion for morphological study. The S powder was kept constant at 120 mg.

Precursor type	**Annealing N_2 pressure (mbar)**	**Annealing temperature (°C)**
Oxide	250, 500, 1000	540
	250	560

Table 2. Overview of the annealing parameters used for CZTS absorbers prepared via the oxide, oxy-sulfide and sulfide routes. All samples were annealed at 580ºC. The S powder was kept constant at 120 mg.

Precursor type	**Annealing N_2 pressure (mbar)**	**Sn powder during annealing (mg)**
Oxide	50, 250, 500, 1000	5
	250	-
Oxy-sulfide	50, 250, 500, 1000	5
	250	-
Sulfide	50, 250, 500, 1000	5
	250	-

3. Results and discussion

3.1 Morphological studies of oxide precursors

The cross-sectional and the top view SEM images of the oxide precursors sulfurized under different conditions are shown in Fig. 1 and Fig. S2, respectively. The elemental composition of the oxide precursors is given in Fig. S1. When oxide samples are annealed under the typical annealing conditions used for sulfide precursors (Fig. 1 (a), 540 °C, 1000 mbar), the films exhibit a high roughness. The image reveals the formation of bubble-like structures and a small-grained layer at the CZTS/Mo interface. By decreasing the N_2 pressure during sulfurization to 500 and 250 mbar as in Fig. 1 (b) and (c), respectively, results in a significant change in morphology and a reduction of the bubble-like features. Furthermore, a small increase in the annealing temperature from 540 °C to 560 °C at 250 mbar results in a more uniform films with larger grains, as shown in Fig. 1 (d). However, the small-grained interface layer persisted even at 560 °C.

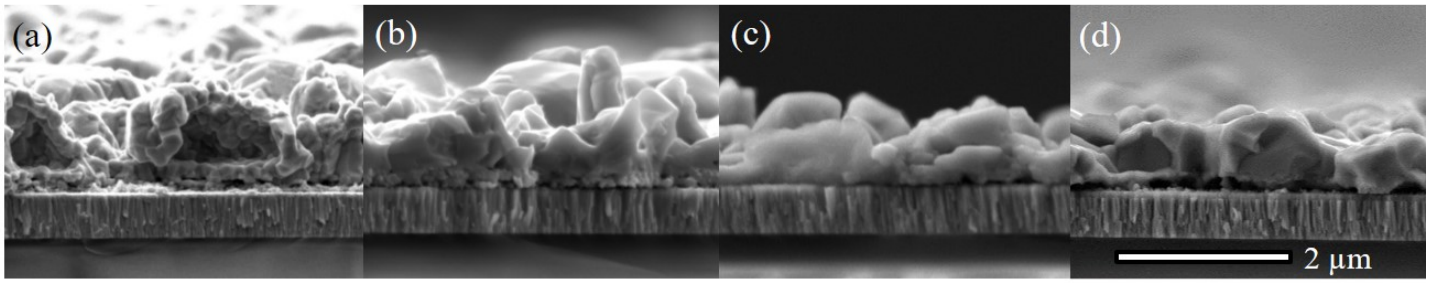

Fig. 1. Cross-sectional SEM images of oxide precursors sulfurized at various temperatures and N_2 pressures: (a) 540 °C, 1000 mbar, (b) 540 °C, 500 mbar, (c) 540 °C, 250 mbar and (d) 560 °C, 250 mbar. The scale bar applies to all images.

In order to understand the formation of the small-grained layer at the back of CZTS, Raman scattering measurements were performed on an oxide precursor annealed on a sapphire substrate (Fig. 2). The oxide precursor was annealed at 250 mbar and 580 °C with 5 mg Sn powder. Raman spectra were measured from the front and back of CZTS (through the sapphire substrate). CZTS, SnS, SnS_2[27–29] and SnO_2 phases were identified at the back of the absorber layer[30–32], while the front surface only shows the CZTS phase. Due to the limited

Raman information depth in CZTS (~100 nm for an excitation wavelength of 532 nm), measurements only show surface local phases[28]. A comparison between Raman spectra "Back 1" and "Back 2" taken at different positions on the backside of CZTS indicate that the tin sulfide/oxide small-grained layer is not continuous. Furthermore, our findings reveal an incomplete sulfurization of the oxide precursors.

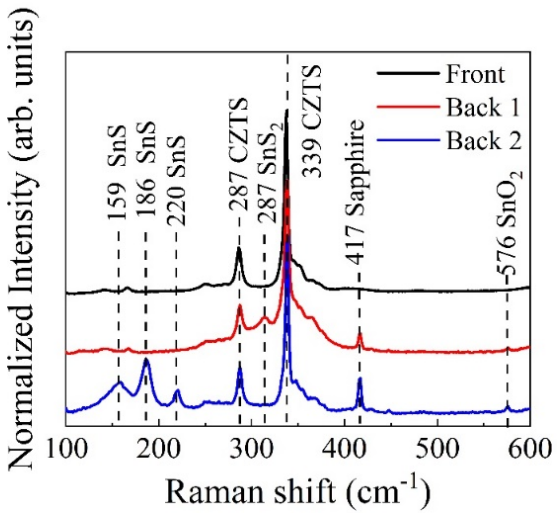

Fig. 2. Raman spectra (λ=532 nm) of CZTS produced from oxide precursor on a sapphire substrate measured from the front (bare absorber surface) and backside (through the sapphire substrate) at two positions.

3.2 Comparison between sulfurization of oxide, oxy-sulfide and sulfide precursors

Fig. 3 shows the cross-sectional SEM images of solar cells based on oxide, oxy-sulfide and sulfide precursors annealed at 250 mbar, 580 °C for 30 min. As the oxygen content in the precursor increases, an increase in grain size is observed. Moreover, the grain size increase is independent of annealing pressure at 580 °C (not shown). Several studies have reported an enhancement in grain size under oxygen-annealing conditions, e.g. by employing open air oxidation of CZTS nanoparticles[33], by adding a MoO_2 layer on the back contact[34], or by adding a Na_2MoO_4 layer on the back contact[35]. The SnO_xS_y layer at the CZTS/Mo interface

is present in oxide and oxy-sulfide samples. The thickness of this layer increases with higher oxygen content in the precursors. For longer thermal exposure during sulfurization, such as 50 min annealing time at temperature of 580 °C, it was possible to eliminate the SnS_xO_y rich layer (Fig. S3).

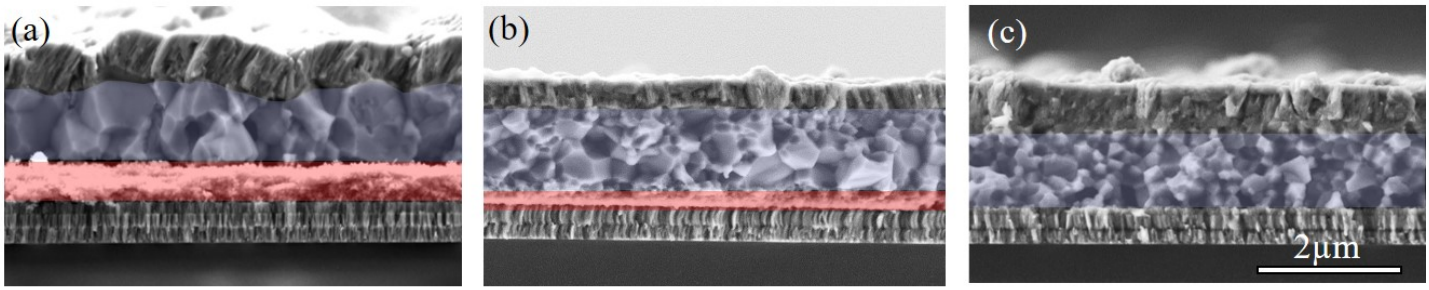

Fig. 3. Cross-sectional SEM images of CZTS solar cells made by oxide (a), oxy-sulfide (b) and sulfide (c) precursors annealed at 250 mbar, 580 °C for 30 min. The CZTS absorber layer (blue) and small grained SnO_xS_y-rich phase (red) are highlighted in colour for visualization purpose. The scale bar applies to all images.

Fig. 4 (a) depicts XRD patterns for the different precursors sulfurized at 1000 mbar, 580 °C for 30 min. In agreement with the Raman data show earlier, CZTS (ICSD 23626), SnO_2 (ICSD 9163) and SnS_xO_y phases were observed. We did not detected any other oxide phases, such as CuO (ICSD 16025), ZnO (ICSD 65120) or Zn_2SnO_4 (ICSD 28235). These results show that SnO_2 is a resilient compound even at 580 °C and the last oxide phase to convert to sulfide. Jin et al. and Chen et al.[14,36] showed that the relative stability of oxide phases increases from CuO to ZnO and finally SnO_2, which is consistent with our results. Increasing the oxygen content in the absorber results in increasing SnO_2 peaks (Fig. 4 (a)). The results support the SEM images in Fig. 3, where the thickness of the small-grained layer at the back contact increases as the oxygen content in the films increases. The low intensity peaks observed in the XRD measurement matches the $Sn_2(S_2O_4)_2$ (ICSD 32684) database. As there are many phases

and structures of SnS_xO_y, XRD diffraction patterns are difficult to analyze. Without Raman measurement (Fig. 2) it would have been difficult to assign SnS_xO_y phases.

The XRD patterns of oxy-sulfide precursors sulfurized at different N_2 pressures are shown in Fig. 4 (b). In the oxy-sulfide series, as the pressure decreases from 1000 mbar to 500 mbar, the SnO_2 peaks become less intense and almost vanish at 250 mbar and 50 mbar, suggesting a more efficient conversion from oxide to sulfide as pressure decreases. One possible explanation for the observed trend is that the SnO_2 converts to SnS_x, as we have seen SnS_x phases in Raman measurements (Fig. 2).

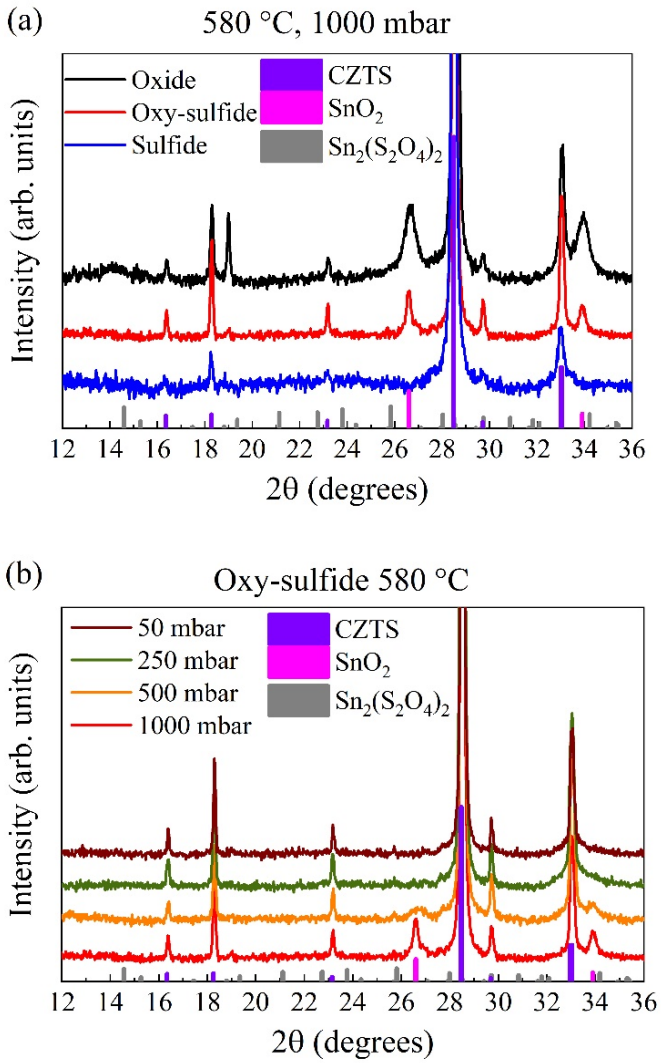

Fig. 4. XRD patterns of oxide, oxy-sulfide and sulfide precursors sulfurized at 1000 mbar (a), and oxy-sulfide precursors sulfurized at 580 °C with different N_2 pressure (b).

Our results indicate that the low pressure of ~ 250 mbar is optimum for the CZTS absorber made from oxide precursor films. In the 50 mbar case, we could not produce good solar cells, probably due to a large composition change in the films after annealing (Fig. S4). As a quaternary compound, the composition of CZTS is sensitive to synthesis conditions. Secondary phases and compositional gradients readily form. The best performing CZTS devices are made with Cu/(Zn+Sn)~0.8 and Zn/Sn~1.2[37]. For sulfide films, we expect that Sn and S are more easily evaporated at lower pressure, which would inherently lead to Cu- and Zn-rich films[38]. On the other hand, for oxide films the more stable SnO_2 is present in the precursor, which could be one of the reason why there is a large difference in composition at 50 mbar. Thus, the optimum annealing conditions for oxide samples are at a temperature of 580 °C, N_2 pressure of 250 mbar and dwelling time of 30 minutes.

3.3 Proposed synthesis routes for the formation of CZTS from oxide and sulfide precursors

We next discuss the synthesis routes for the formation of CZTS from oxide and sulfide precursors. The chemical equilibrium reaction for the sulfide route shown in Eq. (1) was proposed by Redinger et al.[13]. It involves solid phases of Cu_2S and ZnS and volatile gaseous phases of SnS and S_2. They showed that an additional Sn source in the annealing process can boost the performance of the cells, since it accommodates for the volatility of the SnS phase[11,12,39].

$$Cu_2S(s) + ZnS(s) + SnS(g) + \frac{1}{2}S_2(g) \leftrightarrows Cu_2ZnSnS_4(s) \quad (1)$$

$$10CuO(s) + 3ZnO(s) + Zn_2SnO_4(s) + 4SnO_2(s) + \frac{65}{4}S_2(g) \leftrightarrows 5Cu_2ZnSnS_4(s) + \frac{25}{2}SO_2(g) \quad (2)$$

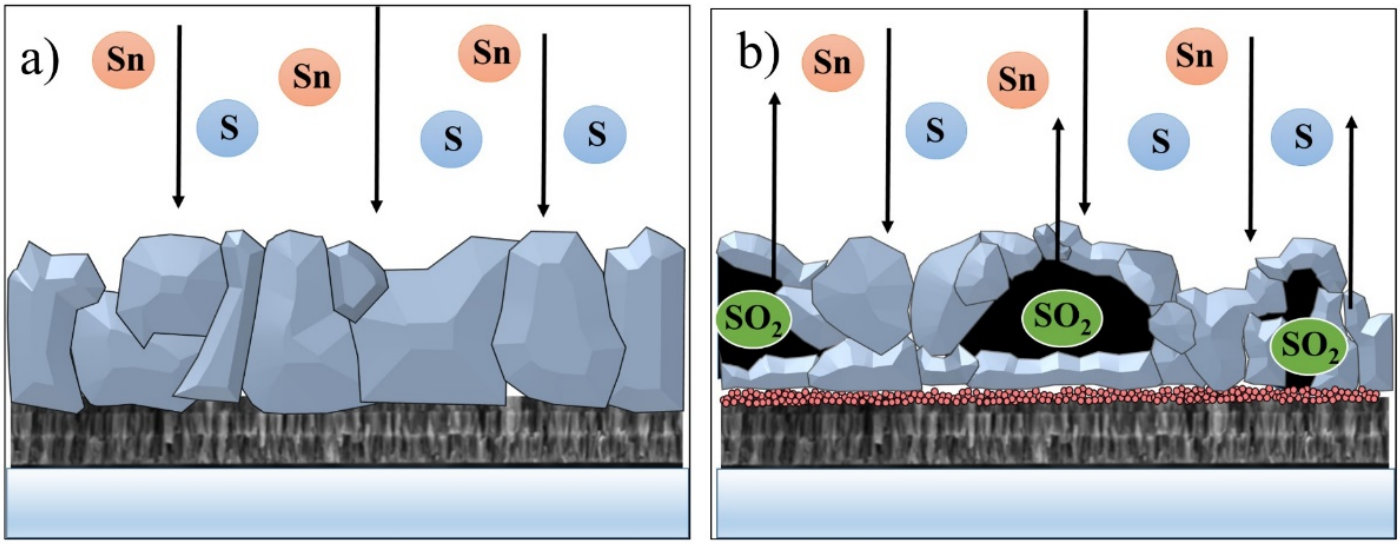

Fig. 5. Proposed synthesis routes for the formation of CZTS from (a) sulfide and (b) oxide precursors.

An illustration of the formation of CZTS via the sulfide route is shown in Fig. 5 (a). According to Jin et al.[14], the equilibrium reaction of the oxide route to CZTS in Eq. (2) involves solid phases of CuO, ZnO, Zn_2SnO_4 and SnO. This route has only one volatile reactant, S_2, which can be compensated by additional sulfur powder during the annealing. However, the oxide-to-sulfide conversion produces SO_2 gas, as depicted in Fig. 5 (b) and Eq. (2).

The formation of bubble-like structures (Fig. 1 (a) and 5 (b)) suggests that SO_2 gas is trapped inside the CZTS film. By lowering the N_2 pressure to 250 mbar during the annealing (Fig. 1 (b,c)), the SO_2 gas may be released at an earlier stage, and thus avoiding the pressure build-up inside the absorber that would inherently lead to the formation of bubbles. The observations are also supported by the XRD data, which show that a low N_2 annealing pressure leads to a lower SnO_2 peak (Fig. 4 (b)). As shown previously, SnO_2 is accumulated at the Mo back contact. By releasing the trapped SO_2 gas, it should become easier to sulfurize SnO_2 as the oxygen source is eliminated. Thus it seems that the SO_2 gas trapped inside the CZTS layer during the sulfurization process is the main reason for the incomplete sulfurization and non-compact surface with bubble-like formations. These formations could potentially lead to shunt paths and increased surface recombination, which degrade device parameters, particularly the fill factor.

There are previous reports on synthesis of $CuInSe_2$ (CIS)[40], $Cu(In,Ga)Se_2$ (CIGS)[40–43], Cu_2SrSnS_4 (CSTS), Cu_2FeSnS_4 (CFTS)[44] and CZTS[14,17] from oxide precursors. The commonly encountered problems were a segregation of the more stable phases such as gallium oxide[41–43,45], the formation of a small-grain layer[40–43,46] as well as voids[40–43,46] at the bottom interface. CFTS has shown increased roughness as annealing temperature increases[44]. The CSTS absorbers made from oxide films have unknown phases at low-temperature sulfurization[46], which resembles the SnO_2 phase in our experiment. Moreover, the films display large, uniform grains, but pinholes appear upon the removal of Na-Sr-Sn-S based secondary phases. Jingjing et al. [47] have reported on the synthesis of $CuIn(S,Se)_2$ from a DMF solution, with absorbers selenized at different Ar pressures. At low pressure (0 MPa), large grains with pinholes and a rough surface were observed. At high pressure (0.06 MPa), large grains without pinholes, but with a small-grain layer and voids at the back contact were observed. Their explanation for the void formation and small-grain layer at the back contact was migration of Cu and In to the surface leaving voids.

It is worth to mention that O/(O+S) ratio in the oxide, oxy-sulfide and sulfide samples were comparable after annealing at 250 mbar when measured by EDX (Table S1). It seems that the oxide samples are completely sulfurized at 250 mbar, or at least they have same O/(O+S) ratio as the sulfide samples. When oxide and oxy-sulfide samples are annealed at pressure above 250 mbar, we see an increased O/(O+S) and bandgap (Fig. S5). This result might indicate CZTSO alloying is possible[18]. However, we have not detected any significant change in XRD and Raman measurements that might show that oxygen alloying is present in the samples.

3.4 **Device characterization**

The J-V curves and EQE spectra of CZTS solar cells produced from precursors sulfurized at 250 mbar, 580 °C are shown in Fig. 6 (a) and (b), respectively. The corresponding device parameters, including open circuit voltage (V_{OC}), short circuit current (J_{SC}), fill factor (FF) and

power conversion efficiency (PCE) are summarized in Table 3. When compared to earlier reports solar cells made by PLD, for example by Jin et al.[15] (PCE = 4.94%, V_{OC} = 0.684 V, J_{SC} = 16.8 mA/cm^2, FF = 43%), our best device has a higher FF. Furthermore, the efficiency of our best device of 5.4% (active area) exceeds that of 5.2% (active area) achieved earlier by our group for PLD of sulfides (V_{OC} = 0.616 V, J_{SC} = 17.6 mA/cm^2, FF = 48%) [48]. In our previous work, an antireflective MgF layer was used, which may account for the larger J_{SC}. Devices made from oxide films annealed at 250 mbar exhibit the highest V_{OC} of 0.673 V, even though the experimentally determined bandgap of 1.52 eV is the lowest among all precursors (Table 3). As a result, the oxide films have the lowest V_{OC} deficit of 0.85 V. We emphasize that the oxides have a better performance because all samples were compared under the best annealing conditions for oxides that are described in section 3.1 and 3.2. The short circuit current values derived from the illuminated J-V curves are in good agreement with those obtained by integration of the EQE curves (see Table 3). Moreover, the EQE is higher below 500 nm in oxides due to a thinner CdS, and thus less absorption will occur in the buffer layer. This suggests that the thickness of the CdS layer can be further optimized.

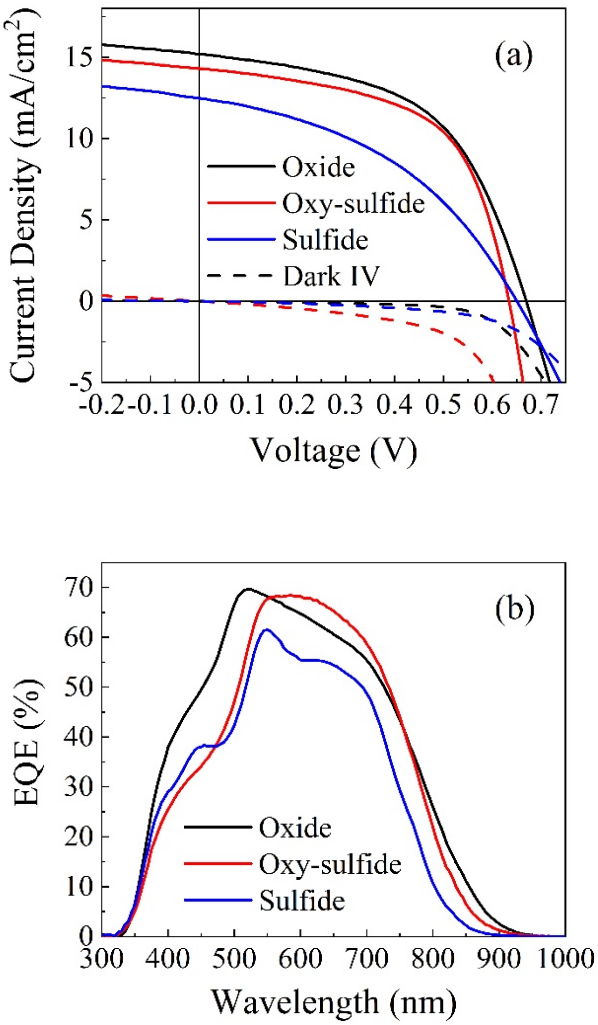

Fig. 6. J-V curves (a) and EQE spectra of the oxide, oxy-sulfide and sulfide cells (b) produced by sulfurization at 250 mbar.

Table 3. J-V parameters of the oxide, oxy-sulfide and sulfide based solar cells produced by sulfurization at 250 mbar.

Precursor type	**J-V parameters**				**EQE**		**V_{OC} deficit (V)**
	V_{OC} (mV)	**J_{SC} (mA/cm^2)**	**FF (%)**	**PCE (%)**	**J_{SC} (mA/cm^2)**	**E_g (eV)**	
Oxide	673	15.2	53.0	5.4	15.5	1.52	0.85
Oxy-sulfide	634	14.3	57.7	5.2	14.4	1.54	0.91

Sulfide	652	12.5	41.9	3.4	12.0	1.59	0.94

Finally, we discuss the effect of both annealing pressure and precursor type on the device performance given by J-V parameters of the best solar cells (Fig. 7). The corresponding J-V curves, EQE spectra and boxplot of all devices made in same condition can be found in the supplementary information (Fig. S6, S7 and S8). The best efficiencies follow the same trend as the median of all data, as can be seen in Fig. S8. Fig. 7 (a) shows that all solar cells have V_{OC} values above 600 mV for oxides, oxy-sulfides and sulfides at different N_2 pressure (except the oxy-sulfide-based solar cell at 50 mbar). However, without Sn powder, the samples annealed at 250 mbar exhibit a drop in V_{OC} by several hundred mV (empty circles in Fig. 7). The poorer performance is most likely associated with a higher density of Sn-related deep level defects in the CZTS absorber[7,37]. The V_{OC} drop is more pronounced for the sulfide device at 250 mbar than for the oxide or oxy-sulfide devices. This could be due to a higher Sn supply in the form of SnS_xO_y in the oxide and oxy-sulfide films. Furthermore, there is a trend of decreasing FF in the absence of Sn during processing, much like V_{OC} (Fig. 7 (a), (c)). The J_{SC} for oxy-sulfide- and sulfide-based solar cells is highest at 500 mbar (Fig. 7 (b)). For solar cells made of oxide precursors, the largest J_{SC} of 15.5 mA/cm^2 is obtained for films annealed at 250 mbar. All devices have J_{SC} values lower than state of the art devices, probably due thicker CdS layer and no antireflection layer. The effect of the small-grained SnS_xO_y-rich layer on device performance is difficult to assign due similar general trends of V_{OC} and J_{SC} observed for different precursors. As a result, for oxide and oxy-sulfide samples, the best performing solar cells were obtained at an annealing pressure of 250 mbar, as expected from the morphological studies of the oxide precursor (Section 3.1)

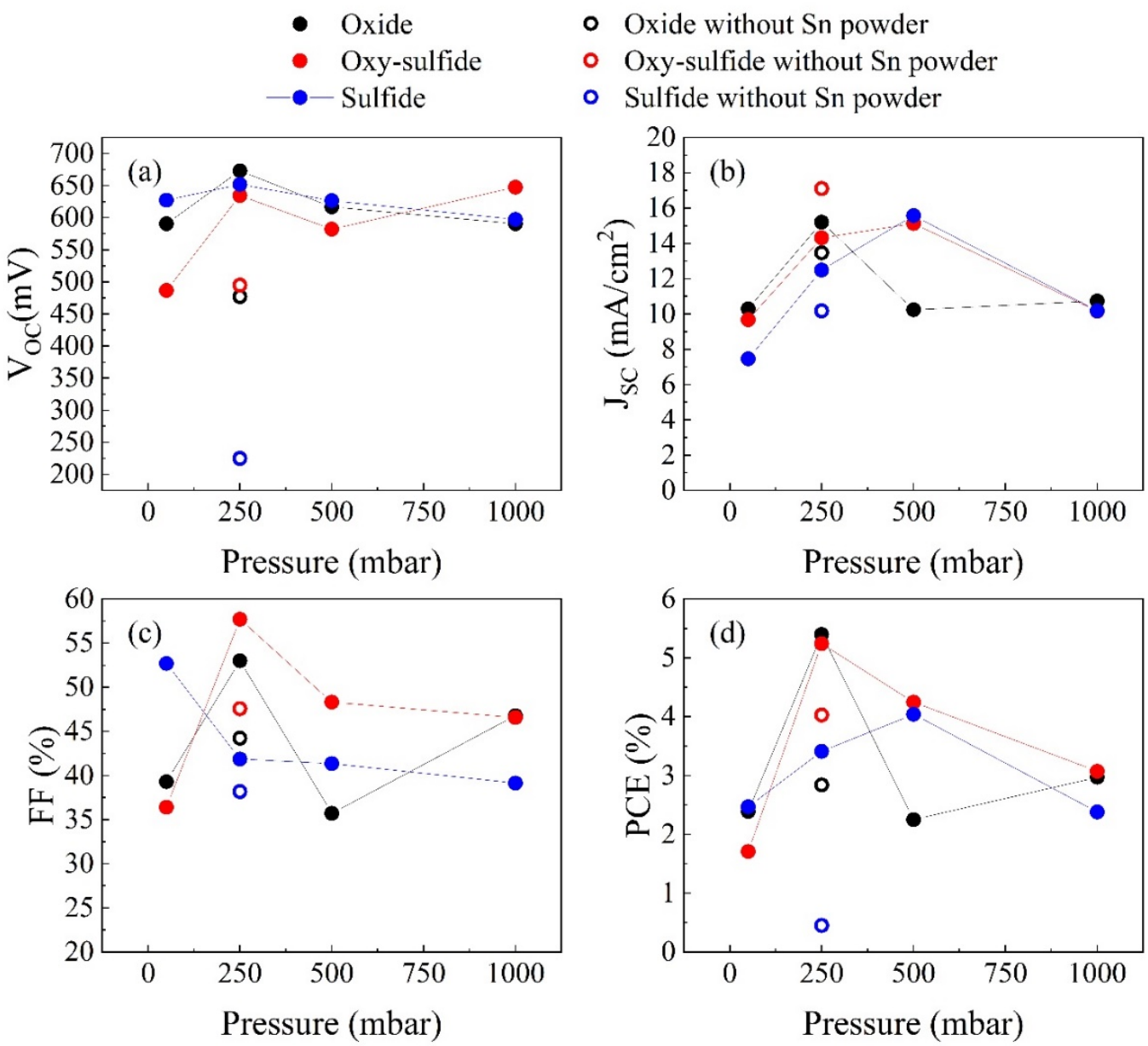

Fig. 7. Device parameters: open circuit voltage (V_{OC}) (a), short circuit current (J_{SC}) (b), fill factor (FF) (c) and power conversion efficiency (PCE) of oxide, oxy-sulfide and sulfide samples at different annealing pressure (d). Samples annealed without Sn powder are shown as empty circles.

4. Conclusion

In conclusion, we have shown that reducing the annealing pressure for the sulfurization of oxide precursors reduces the bubble-like structures and increases the fill factor of CZTS

devices. The rough morphology of CZTS absorbers was associated with SO_2 gas accumulation during the annealing. Reducing the annealing pressure improves the sulfurization process and aids the SO_2 gas release. The optimum annealing pressure for the oxygen-containing precursor films was 250 mbar whereas the sulfide-containing precursors was 500 mbar. SnO_2 is the last compound to convert into a sulfide during the annealing process. SnO_2 was accumulated at the back contact, then converted to SnS_xO_y and finally absorbed by CZTS when Sn supply was needed.

The grain size increased considerably with increasing precursor oxygen content. This increase in grain size was independent on the annealing pressure or on the use of a Sn source during annealing. All oxides fully convert into the sulfide CZTS at a pressure of 250 mbar. Finally, the CZTS solar cells based on oxide precursors have a power conversion efficiency of 5.4%, open circuit voltage of 0.673 V and fill factor of 53%. This stud reports the highest efficiency for CZTS solar cells based on PLD-grown absorbers.

CRediT authorship contribution statement

Mungunshagai Gansukh: Investigation, Visualization, Validation, Methodology, Writing - original draft. **Simón López Mariño**: Investigation, Visualization, Validation, Writing - review & editing. **Moises Espindola Rodriguez**: Investigation, Writing - review & editing. **Sara Lena Josefin Engberg**: Investigation, Writing - review & editing. **Filipe Mesquita Alves Martinho**: Investigation, Writing - review & editing. **Alireza Hajijafarassar**: Investigation. **Niels Christian Schjødt**: Resources. **Eugen Stamate**: Resources. **Ole Hansen:** Resources, Writing - review & editing. **Jørgen Schou**: Resources, Writing - review & editing. **Stela Canulescu**: Writing - review & editing, Supervision. All authors have agreed with the content of the manuscript.

Declaration of competing interest

The authors declare that they have no known competing financial interests or personal relationships that could have appeared to influence the work reported in this paper.

Acknowledgements

This work was supported by the Innovation Fund Denmark through the grant number 6154-00008A.

Appendix A. Supplementary data

The supporting information contains the following seven sections: S1, Elemental analysis of oxide films; S2, Top view SEM images of oxide films described in Table 1; S3, Raman spectra of CZTS; S4, Elemental analysis of absorbers; S5, Band gap and O/(O+S) ratio in oxy-sulfide samples; S6, J-V curves of CZTS solar cells; S7, EQE curves of CZTS solar cells; S8, Boxplot of device parameters; Table S1, O/(O+S) ratio.

References

[1] H. Katagiri, K. Saitoh, T. Washio, H. Shinohara, T. Kurumadani, S. Miyajima, Development of thin film solar cell based on Cu_2ZnSnS_4 thin films, Sol. Energy Mater. Sol. Cells. 65 (2001) 141–148. https://doi.org/10.1016/S0927-0248(00)00088-X.

[2] K. Ito, T. Nakazawa, Electrical and optical properties of stannite-type quaternary semiconductor thin films, Jpn. J. Appl. Phys. 27 (1988) 2094–2097. https://doi.org/10.1143/JJAP.27.2094.

[3] H. Katagiri, K. Jimbo, S. Yamada, T. Kamimura, W.S. Maw, T. Fukano, T. Ito, T.

Motohiro, Enhanced conversion efficiencies of Cu_2ZnSnS_4-based thin film solar cells by using preferential etching technique, Appl. Phys. Express. 1 (2008) 0412011–0412012. https://doi.org/10.1143/APEX.1.041201.

[4] J.J. Scragg, P.J. Dale, L.M. Peter, Synthesis and characterization of Cu_2ZnSnS_4 absorber layers by an electrodeposition-annealing route, Thin Solid Films. 517 (2009) 2481–2484. https://doi.org/10.1016/j.tsf.2008.11.022.

[5] C. Yan, J. Huang, K. Sun, S. Johnston, Y. Zhang, H. Sun, A. Pu, M. He, F. Liu, K. Eder, L. Yang, J.M. Cairney, N.J. Ekins-Daukes, Z. Hameiri, J.A. Stride, S. Chen, M.A. Green, X. Hao, Cu_2ZnSnS_4 solar cells with over 10% power conversion efficiency enabled by heterojunction heat treatment, Nat. Energy. 3 (2018) 764–772. https://doi.org/10.1038/s41560-018-0206-0.

[6] W. Wang, M.T. Winkler, O. Gunawan, T. Gokmen, T.K. Todorov, Y. Zhu, D.B. Mitzi, Device Characteristics of CZTSSe Thin-Film Solar Cells with 12.6% Efficiency, Adv. Energy Mater. 4 (2014) 1301465. https://doi.org/10.1002/aenm.201301465.

[7] S. Kim, J.-S. Park, A. Walsh, Identification of Killer Defects in Kesterite Thin-Film Solar Cells, ACS Energy Lett. 3 (2018) 496–500. https://doi.org/10.1021/acsenergylett.7b01313.

[8] S. Chen, A. Walsh, X.-G. Gong, S.-H. Wei, Classification of Lattice Defects in the Kesterite Cu_2ZnSnS_4 and $Cu_2ZnSnSe_4$ Earth-Abundant Solar Cell Absorbers, Adv. Mater. 25 (2013) 1522–1539. https://doi.org/10.1002/adma.201203146.

[9] S. Bourdais, C. Choné, B. Delatouche, A. Jacob, G. Larramona, C. Moisan, A. Lafond,

F. Donatini, G. Rey, S. Siebentritt, A. Walsh, G. Dennler, Is the Cu/Zn Disorder the Main Culprit for the Voltage Deficit in Kesterite Solar Cells?, Adv. Energy Mater. 6 (2016) 1502276. https://doi.org/10.1002/aenm.201502276.

[10] T. Todorov, D.B. Mitzi, Direct Liquid Coating of Chalcopyrite Light-Absorbing Layers for Photovoltaic Devices, Eur. J. Inorg. Chem. 2010 (2010) 17–28. https://doi.org/10.1002/ejic.200900837.

[11] A. Weber, R. Mainz, H.W. Schock, On the Sn loss from thin films of the material system Cu-Zn-Sn-S in high vacuum, J. Appl. Phys. 107 (2010) 013516. https://doi.org/10.1063/1.3273495.

[12] V. Piacente, S. Foglia, P. Scardala, Sublimation study of the tin sulphides SnS_2, Sn_2S_3 and SnS, J. Alloys Compd. 177 (1991) 17–30. https://doi.org/10.1016/0925-8388(91)90053-X.

[13] A. Redinger, D.M. Berg, P.J. Dale, S. Siebentritt, The consequences of kesterite equilibria for efficient solar cells, J. Am. Chem. Soc. 133 (2011) 3320–3323. https://doi.org/10.1021/ja111713g.

[14] X. Jin, J. Li, G. Chen, C. Xue, W. Liu, C. Zhu, Preparation of Cu_2ZnSnS_4-based thin film solar cells by a combustion method, Sol. Energy Mater. Sol. Cells. 146 (2016) 16–24. https://doi.org/10.1016/j.solmat.2015.11.027.

[15] T. Todorov, L. Oliveira, J. Carda, P. Escribano, Influence of treatment conditions on chalcopyrite films deposited at atmospheric pressure, Phys. Status Solidi. 5 (2008) 3437–3440. https://doi.org/10.1002/pssc.200779441.

[16] T. Washio, T. Shinji, S. Tajima, T. Fukano, T. Motohiro, K. Jimbo, H. Katagiri, 6% Efficiency Cu_2ZnSnS_4-based thin film solar cells using oxide precursors by open atmosphere type CVD, J. Mater. Chem. 22 (2012) 4021–4024. https://doi.org/10.1039/c2jm16454j.

[17] X. Jin, C. Yuan, L. Zhang, G. Jiang, W. Liu, C. Zhu, Pulsed laser deposition of $Cu_2ZnSn(S_xSe_{1-x})_4$ thin film solar cells using quaternary oxide target prepared by combustion method, Sol. Energy Mater. Sol. Cells. 155 (2016) 216–225. https://doi.org/10.1016/j.solmat.2016.06.022.

[18] C. Dun, N.A.W. Holzwarth, Y. Li, W. Huang, D.L. Carroll, $Cu_2ZnSnS_xO_{4-x}$ and $Cu_2ZnSnS_xSe_{4-x}$: First principles simulations of optimal alloy configurations and their energies, J. Appl. Phys. 115 (2014) 193513. https://doi.org/10.1063/1.4876447.

[19] A. Hajijafarassar, F. Martinho, F. Stulen, S. Grini, S. López-Mariño, M. Espíndola-Rodríguez, M. Döbeli, S. Canulescu, E. Stamate, M. Gansukh, S. Engberg, A. Crovetto, L. Vines, J. Schou, O. Hansen, Monolithic thin-film chalcogenide–silicon tandem solar cells enabled by a diffusion barrier, Sol. Energy Mater. Sol. Cells. 207 (2020) 110334. https://doi.org/10.1016/j.solmat.2019.110334.

[20] M. Valentini, C. Malerba, L. Serenelli, M. Izzi, E. Salza, M. Tucci, A. Mittiga, Fabrication of monolithic CZTS/Si tandem cells by development of the intermediate connection, Sol. Energy. 190 (2019) 414–419. https://doi.org/10.1016/j.solener.2019.08.029.

[21] S. Canulescu, E.L. Papadopoulou, D. Anglos, T. Lippert, C.W. Schneider, A. Wokaun, Mechanisms of the laser plume expansion during the ablation of $LiMn_2O_4$, J. Appl.

Phys. 105 (2009) 063107. https://doi.org/10.1063/1.3095687.

[22] S. Canulescu, M. Dobeli, X. Yao, T. Lippert, S. Amoruso, J. Schou, Nonstoichiometric transfer during laser ablation of metal alloys, Phys. Rev. Mater. 1 (2017) 73402. https://doi.org/10.1103/PhysRevMaterials.1.073402.

[23] A. Cazzaniga, A. Crovetto, C. Yan, K. Sun, X. Hao, J. Ramis Estelrich, S. Canulescu, E. Stamate, N. Pryds, O. Hansen, J. Schou, Ultra-thin Cu_2ZnSnS_4 solar cell by pulsed laser deposition, Sol. Energy Mater. Sol. Cells. 166 (2017) 91–99. https://doi.org/10.1016/j.solmat.2017.03.002.

[24] J. Schou, M. Gansukh, R.B. Ettlinger, A. Cazzaniga, M. Grossberg, M. Kauk-Kuusik, S. Canulescu, Pulsed laser deposition of chalcogenide sulfides from multi- and single-component targets: the non-stoichiometric material transfer, Appl. Phys. A Mater. Sci. Process. 124 (2018) 1–7. https://doi.org/10.1007/s00339-017-1475-3.

[25] H. Xie, Y. Sánchez, S. López-Marino, M. Espíndola-Rodríguez, M. Neuschitzer, D. Sylla, A. Fairbrother, V. Izquierdo-Roca, A. Pérez-Rodríguez, E. Saucedo, Impact of Sn(S, Se) Secondary Phases in $Cu_2ZnSn(S, Se)_4$ Solar Cells: a Chemical Route for Their Selective Removal and Absorber Surface Passivation, ACS Appl. Mater. Interfaces. 6 (2014) 12744–12751. https://doi.org/10.1021/am502609c.

[26] A. Crovetto, T.S. Ottsen, E. Stamate, D. Kjær, J. Schou, O. Hansen, On performance limitations and property correlations of Al-doped ZnO deposited by radio-frequency sputtering, J. Phys. D. Appl. Phys. 49 (2016) 295101. https://doi.org/10.1088/0022-3727/49/29/295101.

[27] X. Fontane, V. Izquierdo-Roca, A. Fairbrother, M. Espindola-Rodriguez, S. Lopez-Marino, M. Placidi, T. Jawhari, E. Saucedo, A. Perez-Rodriguez, Selective detection of secondary phases in $Cu_2ZnSn(S, Se)_4$ based absorbers by pre-resonant Raman spectroscopy, in: Conf. Rec. IEEE Photovolt. Spec. Conf., Institute of Electrical and Electronics Engineers Inc., 2013: pp. 2581–2584. https://doi.org/10.1109/PVSC.2013.6745001.

[28] D.M. Berg, M. Arasimowicz, R. Djemour, L. Gütay, S. Siebentritt, S. Schorr, X. Fontané, V. Izquierdo-Roca, A. Pérez-Rodriguez, P.J. Dale, Discrimination and detection limits of secondary phases in Cu_2ZnSnS_4 using X-ray diffraction and Raman spectroscopy, Thin Solid Films. 569 (2014) 113–123. https://doi.org/10.1016/j.tsf.2014.08.028.

[29] L.S. Price, I.P. Parkin, A.M.E. Hardy, R.J.H. Clark, T.G. Hibbert, K.C. Molloy, Atmospheric pressure chemical vapor deposition of tin sulfides (SnS, Sn_2S_3, and SnS_2) on glass, Chem. Mater. 11 (1999) 1792–1799. https://doi.org/10.1021/cm990005z.

[30] T.H. Li, L.Z. Liu, X.X. Li, X.L. Wu, H.T. Chen, P.K. Chu, Oxygen vacancy density-dependent transformation from infrared to Raman active vibration mode in SnO_2 nanostructures, Opt. Lett. 36 (2011) 4296. https://doi.org/10.1364/ol.36.004296.

[31] L.Z. Liu, X.L. Wu, F. Gao, J.C. Shen, T.H. Li, P.K. Chu, Determination of surface oxygen vacancy position in SnO_2 nanocrystals by Raman spectroscopy, Solid State Commun. 151 (2011) 811–814. https://doi.org/10.1016/j.ssc.2011.03.029.

[32] S. Yang, Z. Wu, L.P. Huang, B. Zhou, M. Lei, L. Sun, Q. Tian, J. Pan, W. Wu, H. Zhang, Significantly enhanced dye removal performance of hollow tin oxide

nanoparticles via carbon coating in dark environment and study of its mechanism, Nanoscale Res. Lett. 9 (2014) 1–9. https://doi.org/10.1186/1556-276X-9-442.

[33] S. Exarhos, E. Palmes, R. Xu, L. Mangolini, Oxide-induced grain growth in CZTS nanoparticle coatings, RSC Adv. 7 (2017) 25575–25581. https://doi.org/10.1039/c7ra04128d.

[34] S. Lopez-Marino, M. Espíndola-Rodríguez, Y. Sánchez, X. Alcobé, F. Oliva, H. Xie, M. Neuschitzer, S. Giraldo, M. Placidi, R. Caballero, V. Izquierdo-Roca, A. Pérez-Rodríguez, E. Saucedo, The importance of back contact modification in $Cu_2ZnSnSe_4$ solar cells: The role of a thin MoO_2 layer, Nano Energy. 26 (2016) 708–721. https://doi.org/10.1016/J.NANOEN.2016.06.034.

[35] S. López-Marino, Y. Sánchez, M. Espíndola-Rodríguez, X. Alcobé, H. Xie, M. Neuschitzer, I. Becerril, S. Giraldo, M. Dimitrievska, M. Placidi, L. Fourdrinier, V. Izquierdo-Roca, A. Pérez-Rodríguez, E. Saucedo, Alkali doping strategies for flexible and light-weight $Cu_2ZnSnSe_4$ solar cells, J. Mater. Chem. A. 4 (2016) 1895–1907. https://doi.org/10.1039/C5TA09640E.

[36] G. Chen, C. Yuan, J. Liu, Z. Huang, S. Chen, W. Liu, G. Jiang, C. Zhu, Fabrication of Cu_2ZnSnS_4 thin films using oxides nanoparticles ink for solar cell, J. Power Sources. 276 (2015) 145–152. https://doi.org/10.1016/j.jpowsour.2014.11.112.

[37] S. Chen, A. Walsh, X.-G. Gong, S.-H. Wei, S. Chen, S.-H. Wei, X.-G. Gong, A. Walsh, Classification of Lattice Defects in the Kesterite Cu_2ZnSnS_4 and $Cu_2ZnSnSe_4$ Earth-Abundant Solar Cell Absorbers, Adv. Mater. 25 (2013) 1522–1539. https://doi.org/10.1002/adma.201203146.

[38] P.W. Guan, S.L. Shang, G. Lindwall, T. Anderson, Z.K. Liu, Phase stability of the Cu-Sn-S system and optimal growth conditions for earth-abundant Cu_2SnS_3 solar materials, Sol. Energy. 155 (2017) 745–757. https://doi.org/10.1016/j.solener.2017.07.017.

[39] J.J. Scragg, T. Ericson, T. Kubart, M. Edoff, C. Platzer-Bj, Chemical Insights into the Instability of Cu_2ZnSnS_4 Films during Annealing, Chem. Mater. 23 (2011) 4625–4633. https://doi.org/10.1021/cm202379s.

[40] M. Kaelin, D. Rudmann, F. Kurdesau, T. Meyer, H. Zogg, A.N. Tiwari, CIS and CIGS layers from selenized nanoparticle precursors, in: Thin Solid Films, Elsevier, 2003: pp. 58–62. https://doi.org/10.1016/S0040-6090(03)00194-9.

[41] A. Duchatelet, T. Sidali, N. Loones, G. Savidand, E. Chassaing, D. Lincot, 12.4% Efficient Cu(In,Ga)Se_2 solar cell prepared from one step electrodeposited Cu-In-Ga oxide precursor layer, Sol. Energy Mater. Sol. Cells. 119 (2013) 241–245. https://doi.org/10.1016/j.solmat.2013.07.053.

[42] L. Ribeaucourt, G. Savidand, D. Lincot, E. Chassaing, Electrochemical study of one-step electrodeposition of copper-indium- gallium alloys in acidic conditions as precursor layers for Cu(In,Ga)Se_2 thin film solar cells, Electrochim. Acta. 56 (2011) 6628–6637. https://doi.org/10.1016/j.electacta.2011.05.033.

[43] L. Ribeaucourt, E. Chassaing, G. Savidand, D. Lincot, Synthesis of Cu(In,Ga)Se_2 absorber using one-step electrodeposition of Cu-In-Ga precursor, in: Thin Solid Films, Elsevier, 2011: pp. 7241–7244. https://doi.org/10.1016/j.tsf.2010.12.104.

[44] G. Chen, J. Li, S. Chen, Z. Huang, M. Wu, J. Zhao, W. Wang, H. Lin, C. Zhu, Low cost oxide-based deposition of Cu_2FeSnS_4 thin films for photovoltaic absorbers, Mater. Chem. Phys. 188 (2017) 95–99. https://doi.org/10.1016/j.matchemphys.2016.12.024.

[45] T. Todorov, L. Oliveira, J. Carda, P. Escribano, Influence of treatment conditions on chalcopyrite films deposited at atmospheric pressure, Phys. Status Solidi. 5 (2008) 3437–3440. https://doi.org/10.1002/pssc.200779441.

[46] A. Crovetto, R. Nielsen, E. Stamate, O. Hansen, B. Seger, I. Chorkendorff, P.C.K. Vesborg, Wide Band Gap Cu_2SrSnS_4 Solar Cells from Oxide Precursors, ACS Appl. Energy Mater. 2 (2019) 7340–7344. https://doi.org/10.1021/acsaem.9b01322.

[47] J. Jiang, S. Yu, Y. Gong, W. Yan, R. Zhang, S. Liu, W. Huang, H. Xin, 10.3% Efficient $CuIn(S,Se)_2$ Solar Cells from DMF Molecular Solution with the Absorber Selenized under High Argon Pressure, Sol. RRL. 2 (2018) 1800044. https://doi.org/10.1002/solr.201800044.

[48] A. Cazzaniga, A. Crovetto, C. Yan, K. Sun, X. Hao, J. Ramis Estelrich, S. Canulescu, E. Stamate, N. Pryds, O. Hansen, J. Schou, Ultra-thin Cu_2ZnSnS_4 solar cell by pulsed laser deposition, Sol. Energy Mater. Sol. Cells. 166 (2017) 91–99. https://doi.org/10.1016/j.solmat.2017.03.002.

Figure 1

Click here to download high resolution image

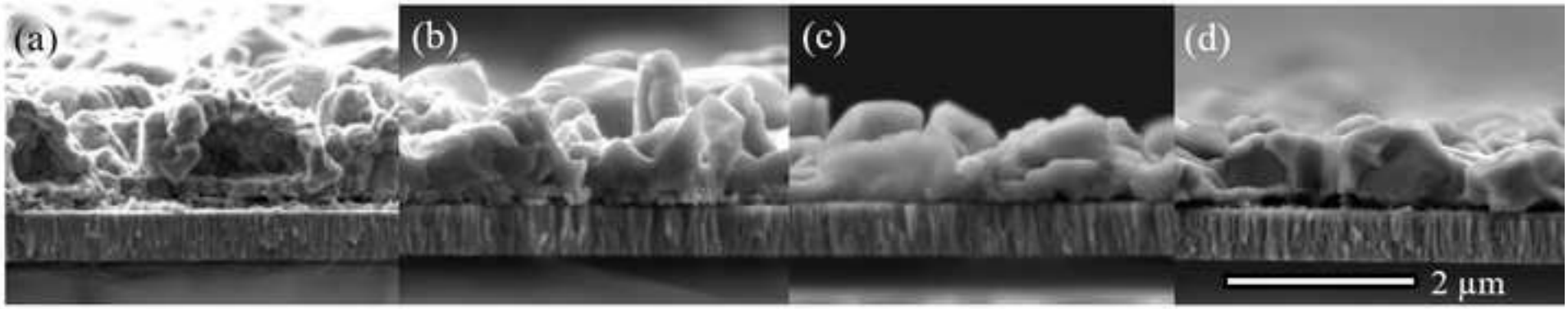

(540 °C, 1000 mbar) (540 °C, 500 mbar) (540 °C, 250 mbar) (560 °C, 250 mbar)

Figure 2

Click here to download high resolution image

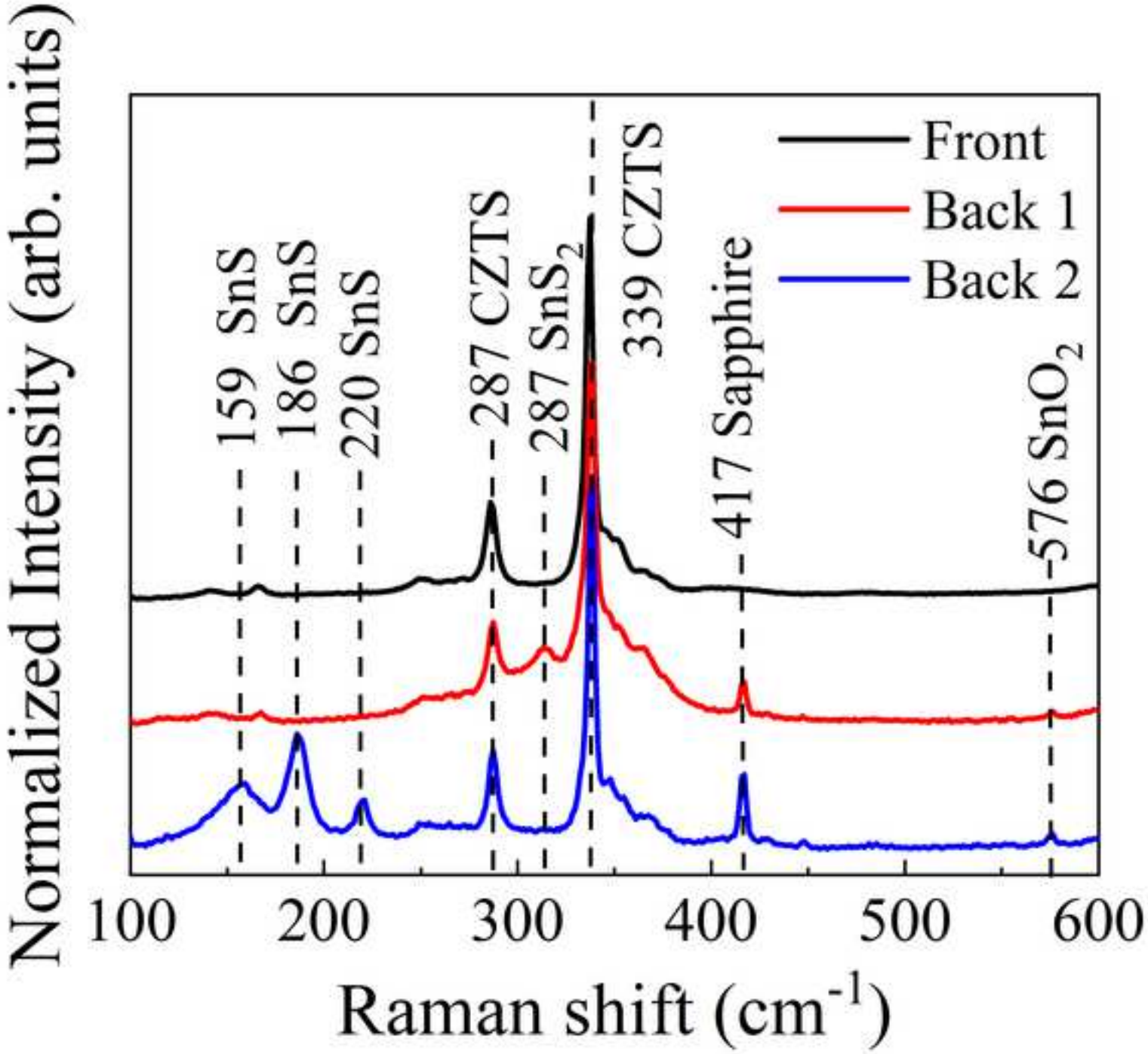

Figure 3

Click here to download high resolution image

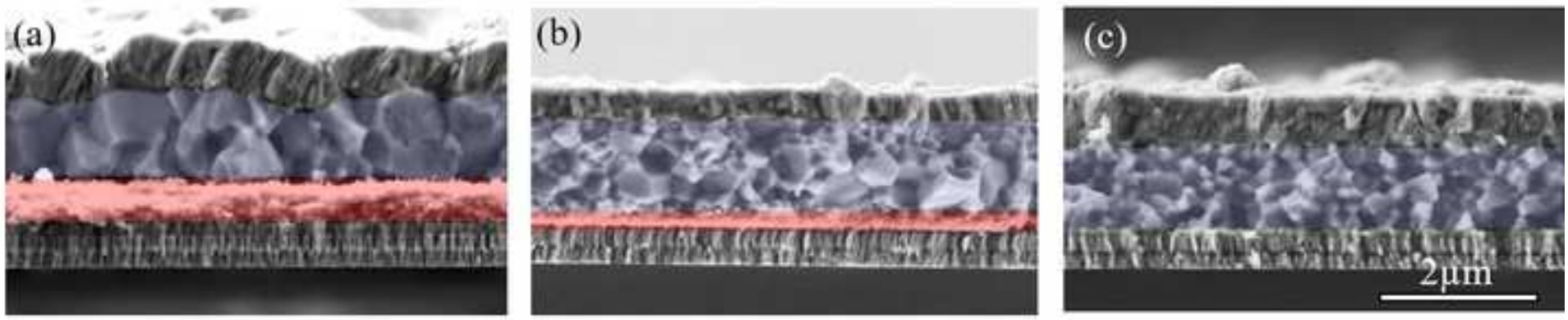

Figure 4a
Click here to download high resolution image

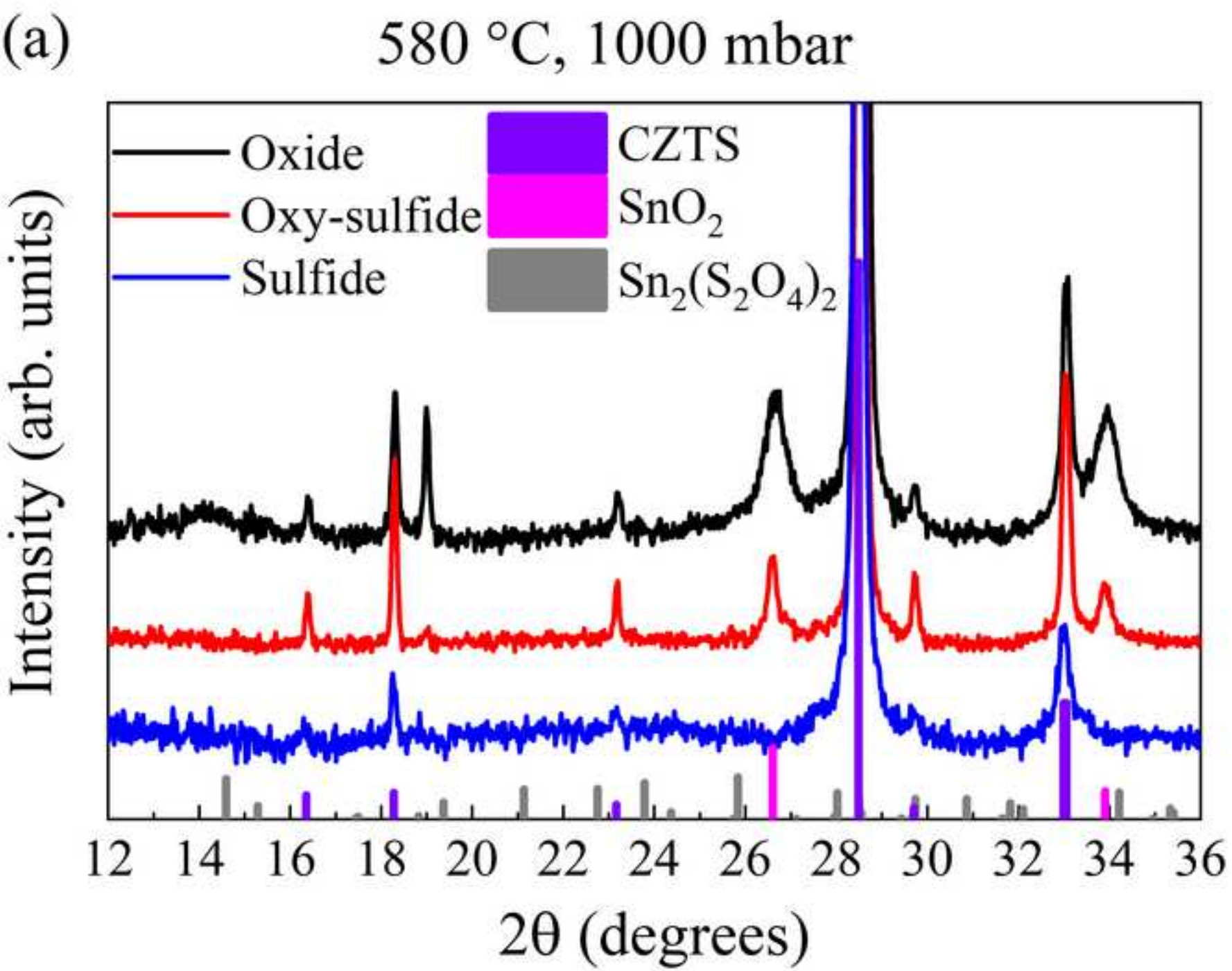

Figure 4b
Click here to download high resolution image

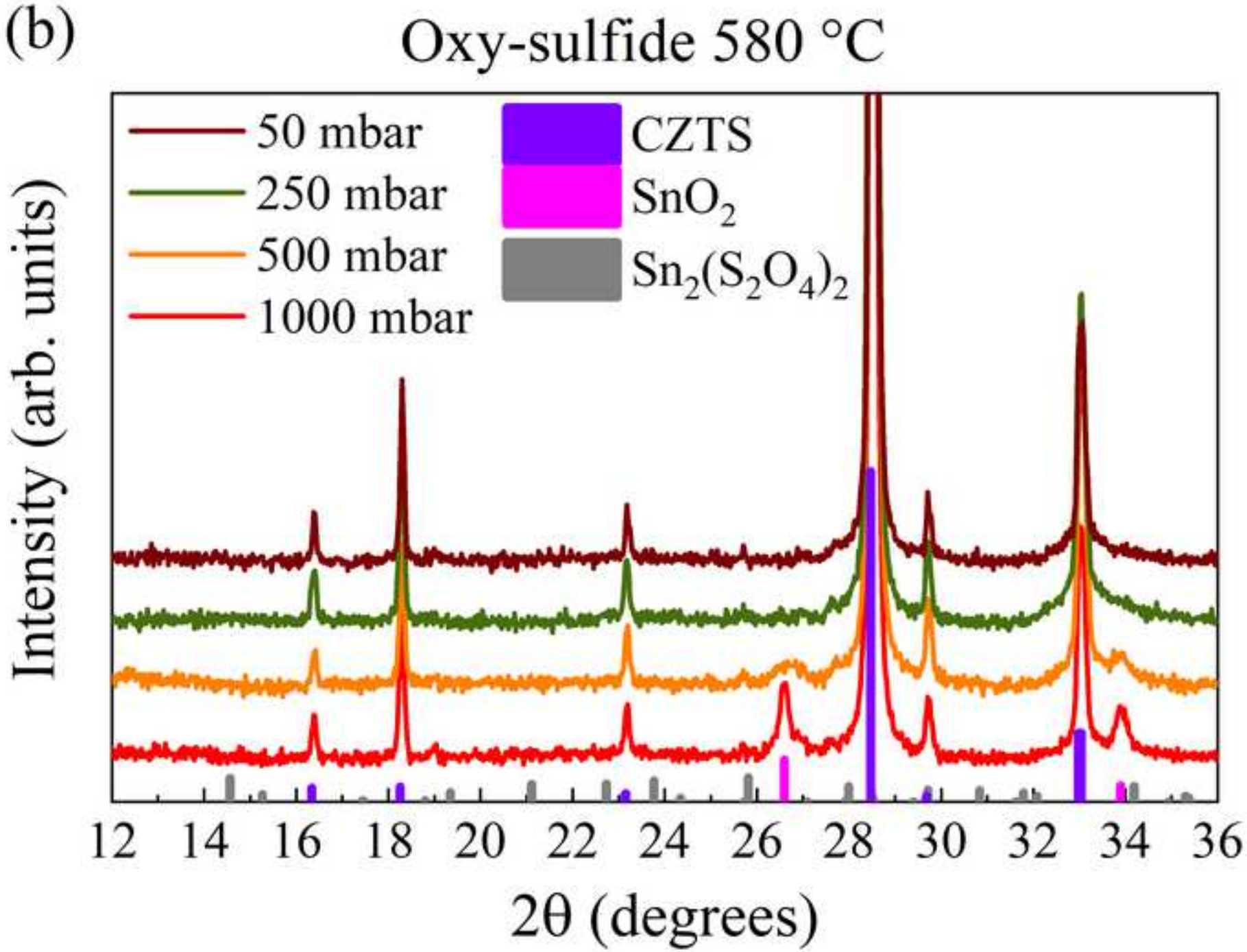

Figure 5

Click here to download high resolution image

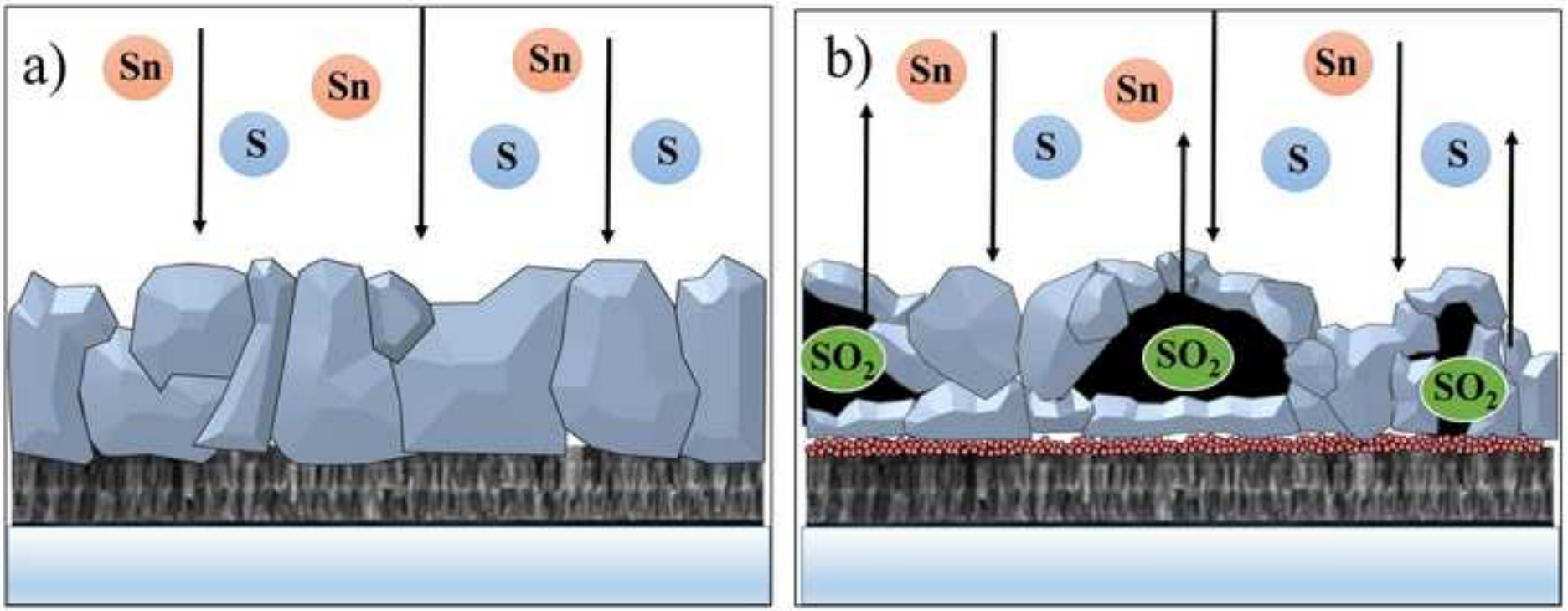

Figure 6a

Click here to download high resolution image

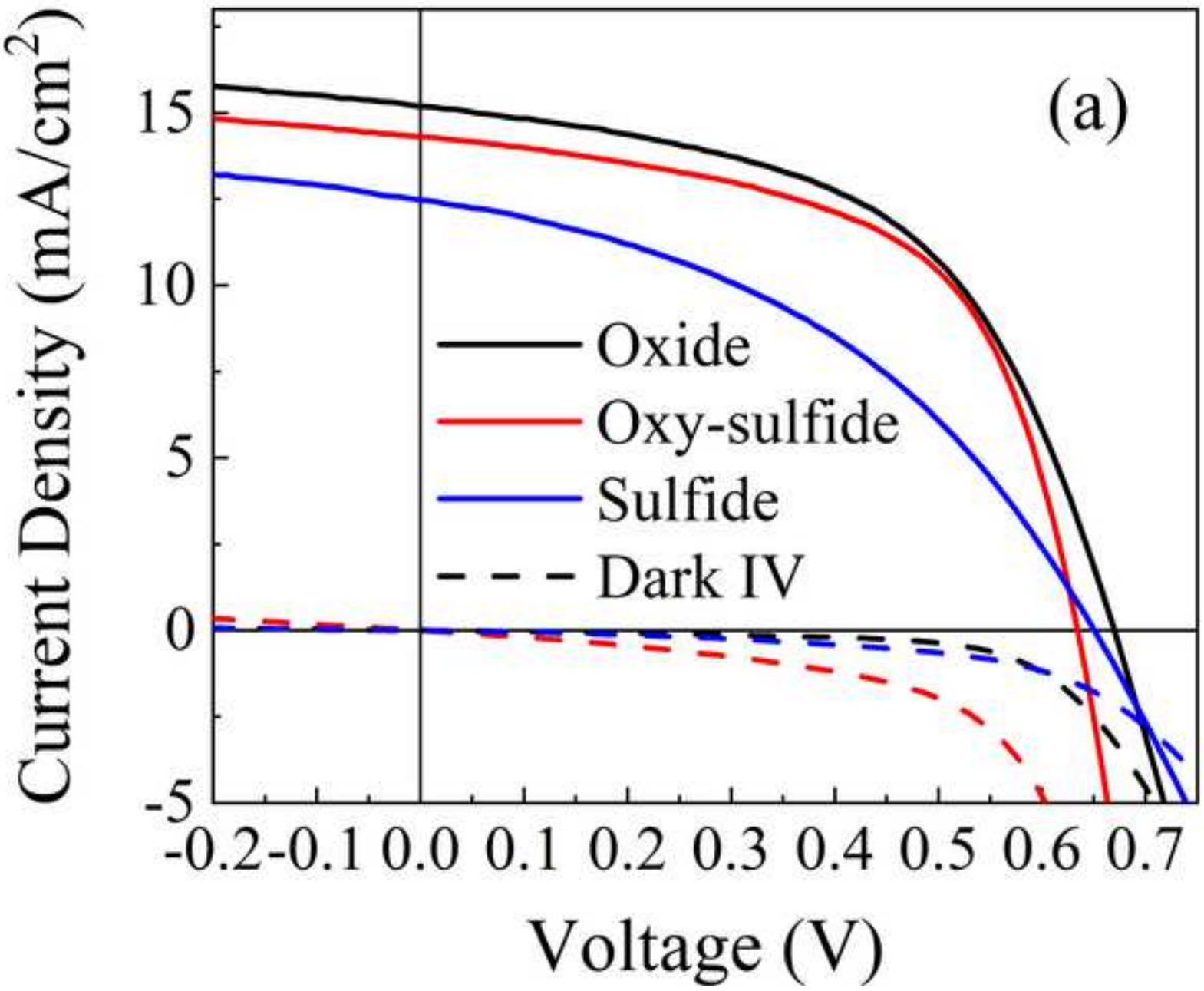

Figure 6b
Click here to download high resolution image

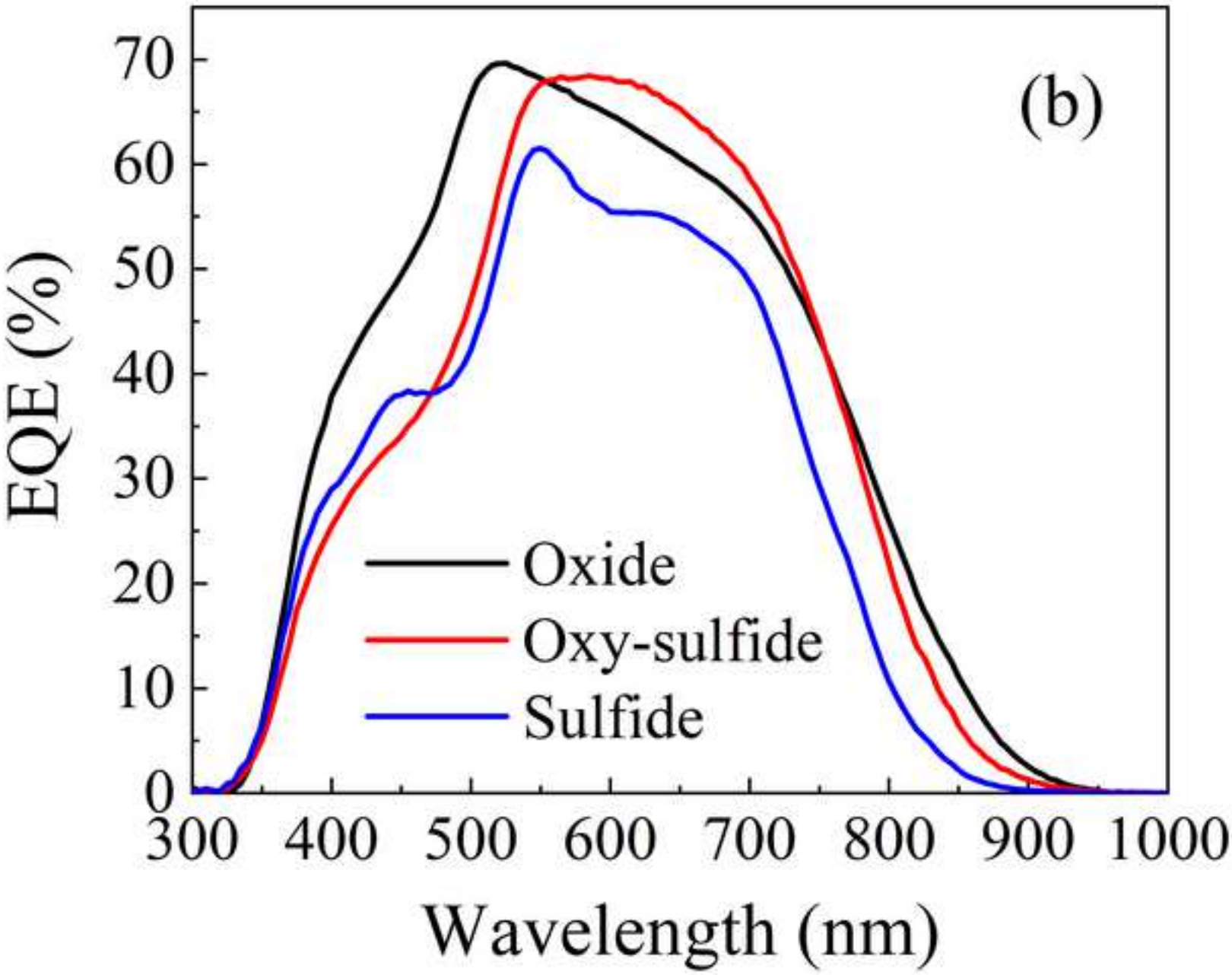

Figure 7

Click here to download high resolution image

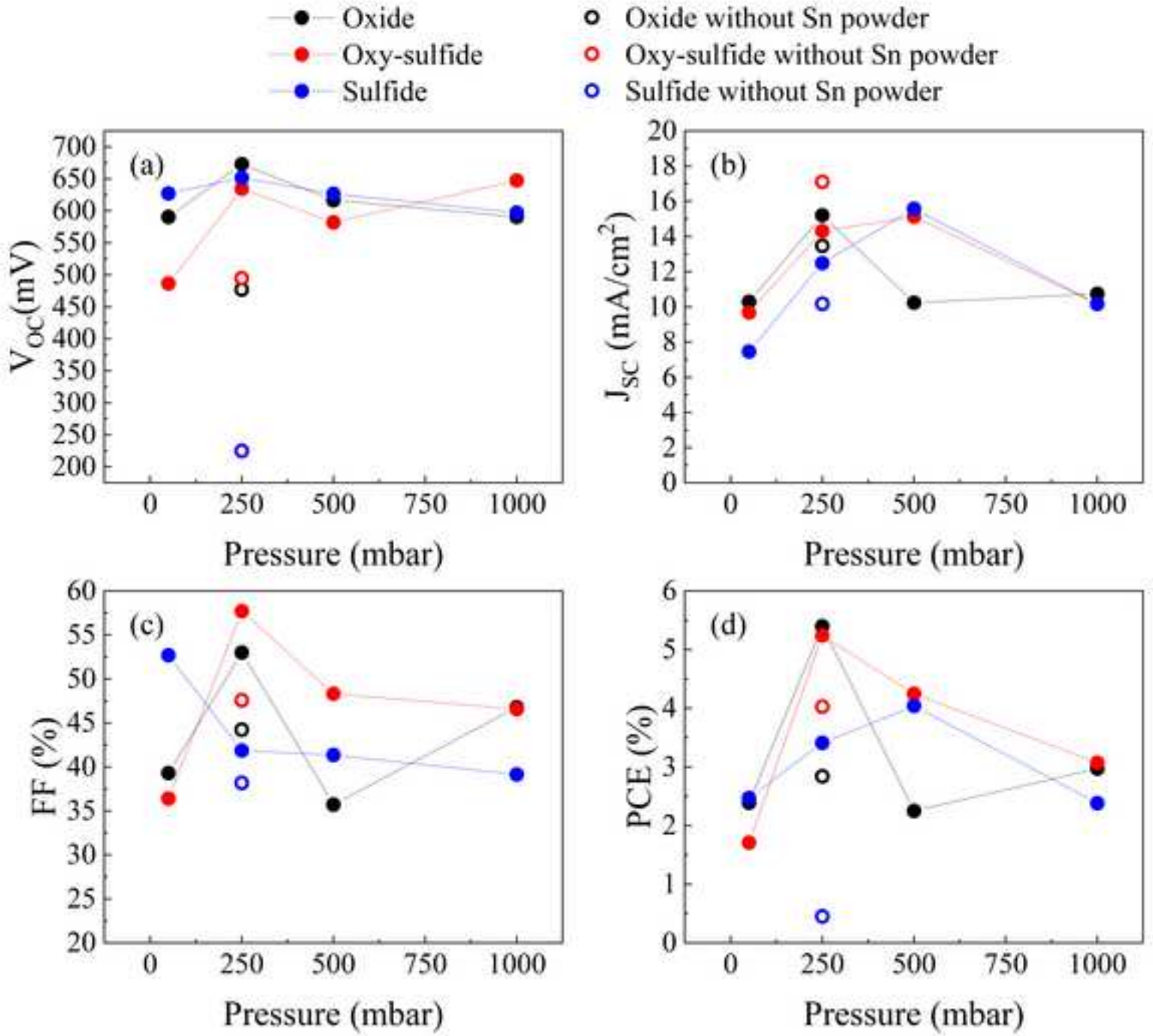

***Credit Author Statement**

Use always full names and complete CRediT authorship contribution statement according to the example given below

Mungunshagai Gansukh[1], Simón López Mariño[2], Moises Espindola Rodriguez[3], Sara Lena Josefin Engberg[1], Filipe Mesquita Alves Martinho[1], Alireza Hajijafarassar[2], Niels Christian Schjødt[4], Eugen Stamate[2], Ole Hansen[2], Jørgen Schou[1] and Stela Canulescu[1]*

CRediT authorship contribution statement

Mungunshagai Gansukh: Conceptualization, Investigation, Formal analysis, Methodology, Writing - original draft. Simón López Mariño: Investigation, Visualization, Validation, Writing - review & editing. Moises Espindola Rodriguez: Investigation, Writing - review & editing. Sara Lena Josefin Engberg: Investigation, Writing - review & editing. Filipe Mesquita Alves Martinho: Investigation, Writing - review & editing. Alireza Hajijafarassar: Investigation. Niels Christian Schjødt: Resources. Eugen Stamate: Resources. Ole Hansen: Resources, Writing - review & editing, Project administration. Jørgen Schou: Resources, Writing - review & editing, Project administration. Stela Canulescu: Writing - review & editing, Project administration, Supervision.

***Declaration of Interest Statement**

Declaration of interests

☒ The authors declare that they have no known competing financial interests or personal relationships that could have appeared to influence the work reported in this paper.

☐The authors declare the following financial interests/personal relationships which may be considered as potential competing interests:

Oxide route for production of Cu_2ZnSnS_4 solar cells by Pulsed Laser Deposition

Mungunshagai Gansukh[1], Simón López Mariño[2], Moises Espindola Rodriguez [3], Sara Lena Josefin Engberg[1], Filipe Mesquita Alves Martinho[1], Alireza Hajijafarassar[2], Niels Christian Schjødt[4], Eugen Stamate[2], Ole Hansen[2], Jørgen Schou[1] and Stela Canulescu[1]*

[1] Department of Photonics Engineering, Technical University of Denmark, DK-4000 Roskilde, Denmark

[2] DTU Nanolab, National Center for Nano Fabrication and Characterization, Technical University of Denmark, DK-2800 Kgs. Lyngby, Denmark

[3] Department of Energy Conversion and Storage, Technical University of Denmark, DK-2800 Kgs. Lyngby, Denmark

[4] Haldor Topsøe A/S, Haldor Topsøes Allé 1, DK-2800 Kgs. Lyngby, Denmark

[*]Corresponding author Stela Canulescu, email: stec@fotonik.dtu.dk

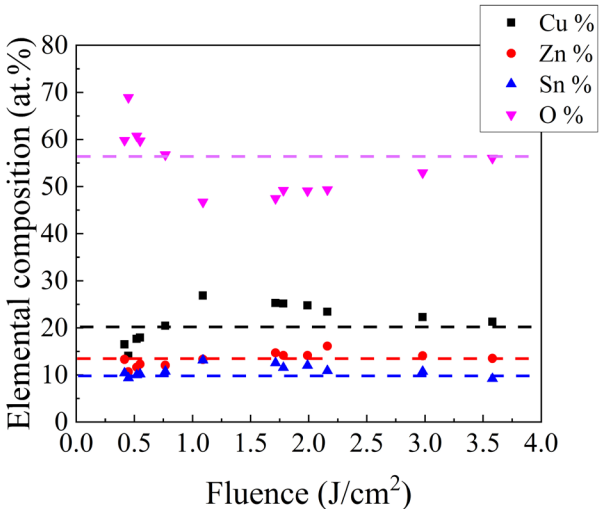

Fig. S1. Elemental composition (at%) of the oxide precursors as a function of the laser fluence, as measured by EDX. Dashed lines indicate the elemental composition of the PLD oxide target. All films were grown on Mo/SLG substrates.

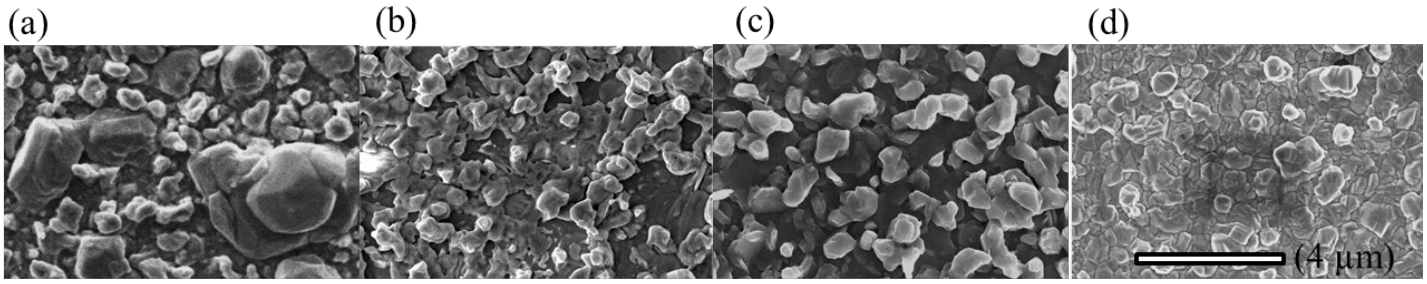

Fig. S2. The top view SEM images of oxide precursors sulfurized at various temperatures and N_2 pressures: (a) 540 °C, 1000 mbar, (b) 540 °C, 500 mbar, (c) 540 °C, 250 mbar and (d) 560 °C, 250 mbar. The scalebar applies to all images.

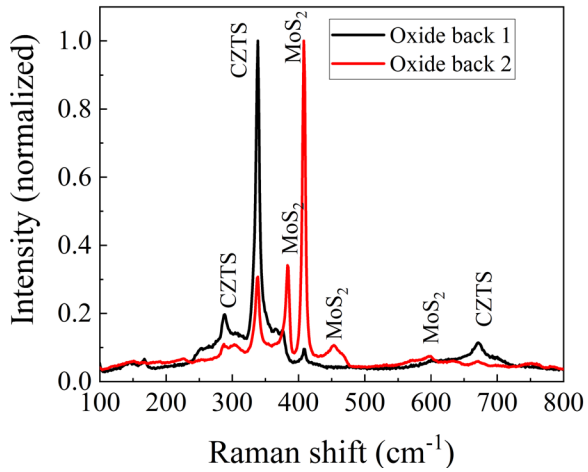

Fig. S3. Raman spectra measured on the back side of the CZTS cell after it has been peeled off from the substrate showing regions of CZTS (oxide back 1) and bulk MoS_2 only (oxide back 2). The CZTS cell is based on oxide precursor annealed at 580°C for 50 minutes.

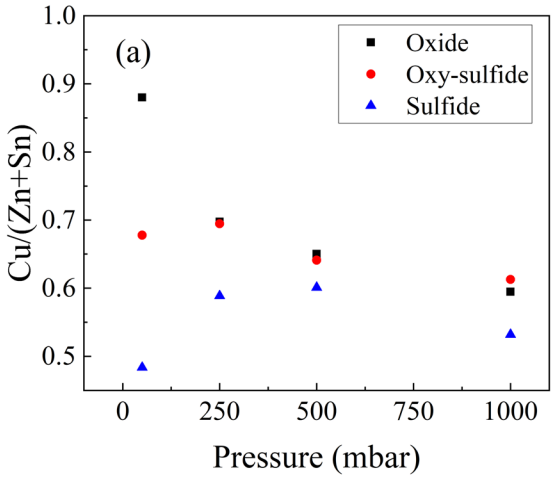

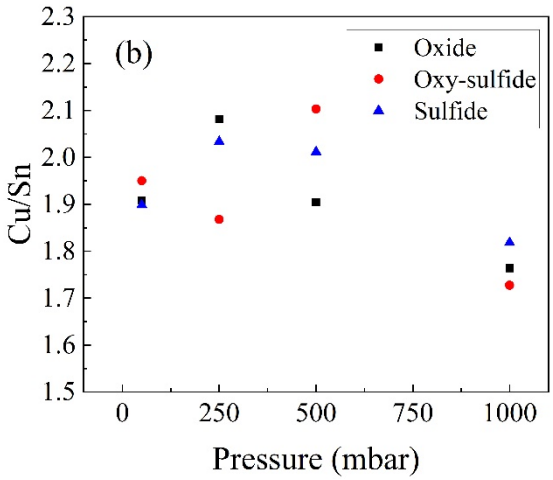

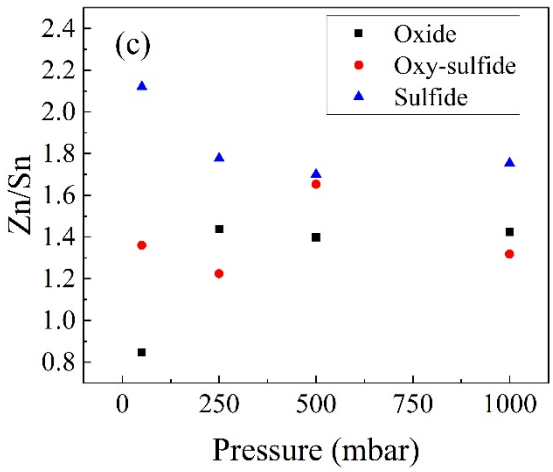

Fig. S4. EDX measurements of different precursors after sulfurization at different N_2 pressures.

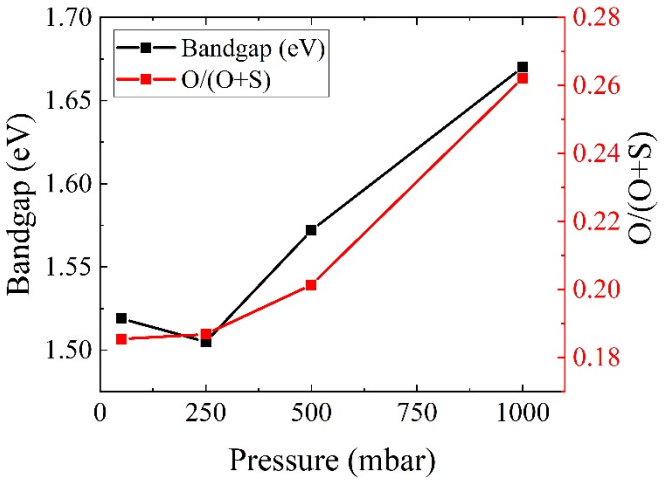

Fig. S5. Bandgap (left-axis) and O/(O+S) ratio (right-axis) of oxy-sulfide samples annealed at different pressures. The band gap and composition were determined by EQE and EDX, respectively.

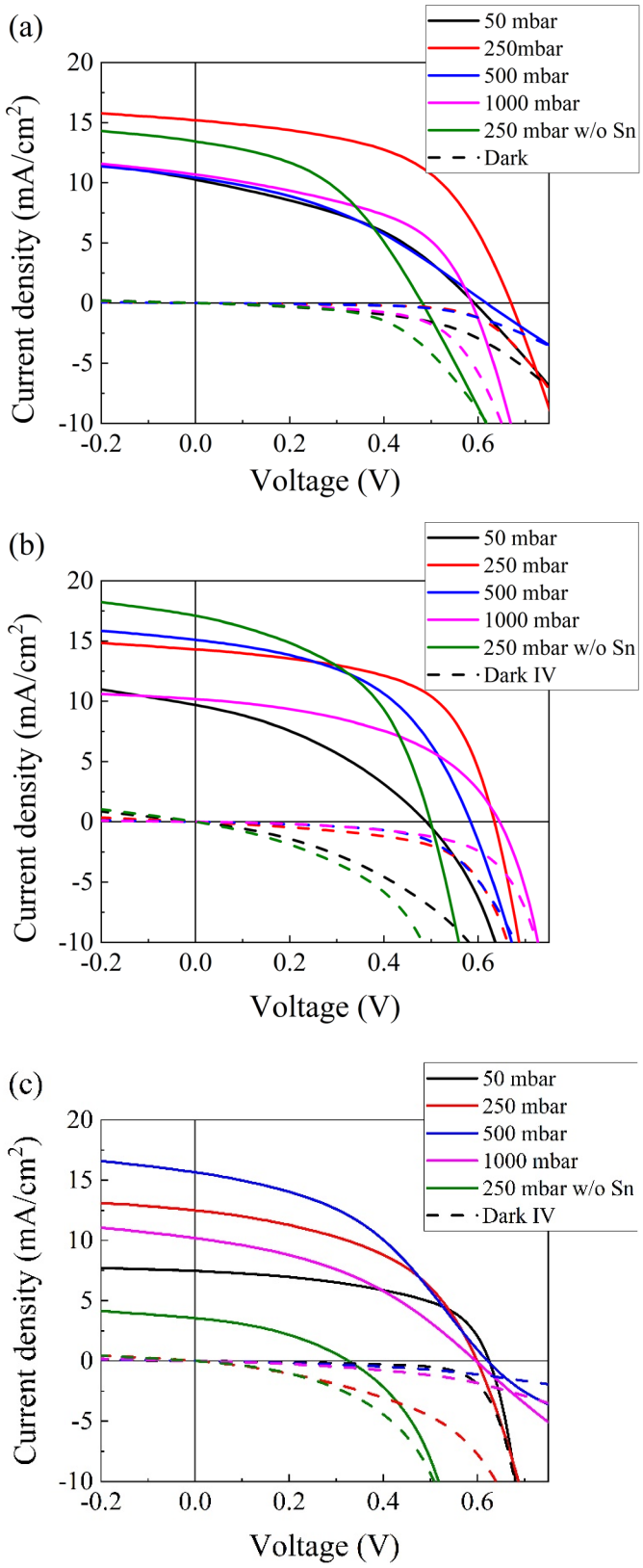

Fig. S6. J-V curves of the best cells based on (a) oxides, (b) oxy-sulfides and (c) sulfides.

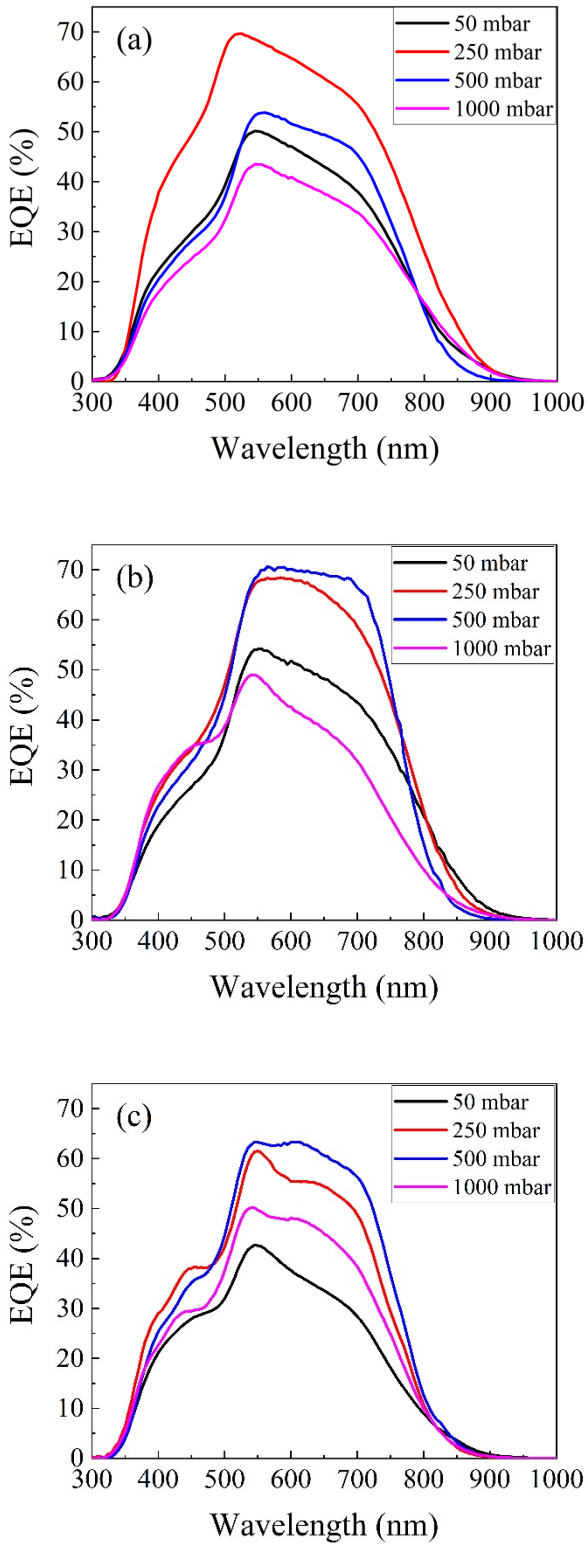

Fig. S7. EQE curves of solar cells made from (a) oxides, (b) oxy-sulfides and (c) sulfides.

Fig. S7 shows EQE measurements on solar cells made from precursors sulfurized at different N_2 pressures. Fig. S6 (a), (b) and (c) correspond to cells made from oxide, oxy-sulfide and sulfide precursors, respectively. For the oxy-sulfide and sulfide samples, the EQE response reaches maximum

at 500 mbar (Fig. S6 (b), (c)). For oxide samples, the EQE reaches its maximum at 250 mbar (Fig. 6 (a),(b)) which resulted in their highest J_{SC}. Sulfide samples have fringes in their EQE response. This could indicate that they are more flat and uniform than oxide and oxy-sulfide samples.

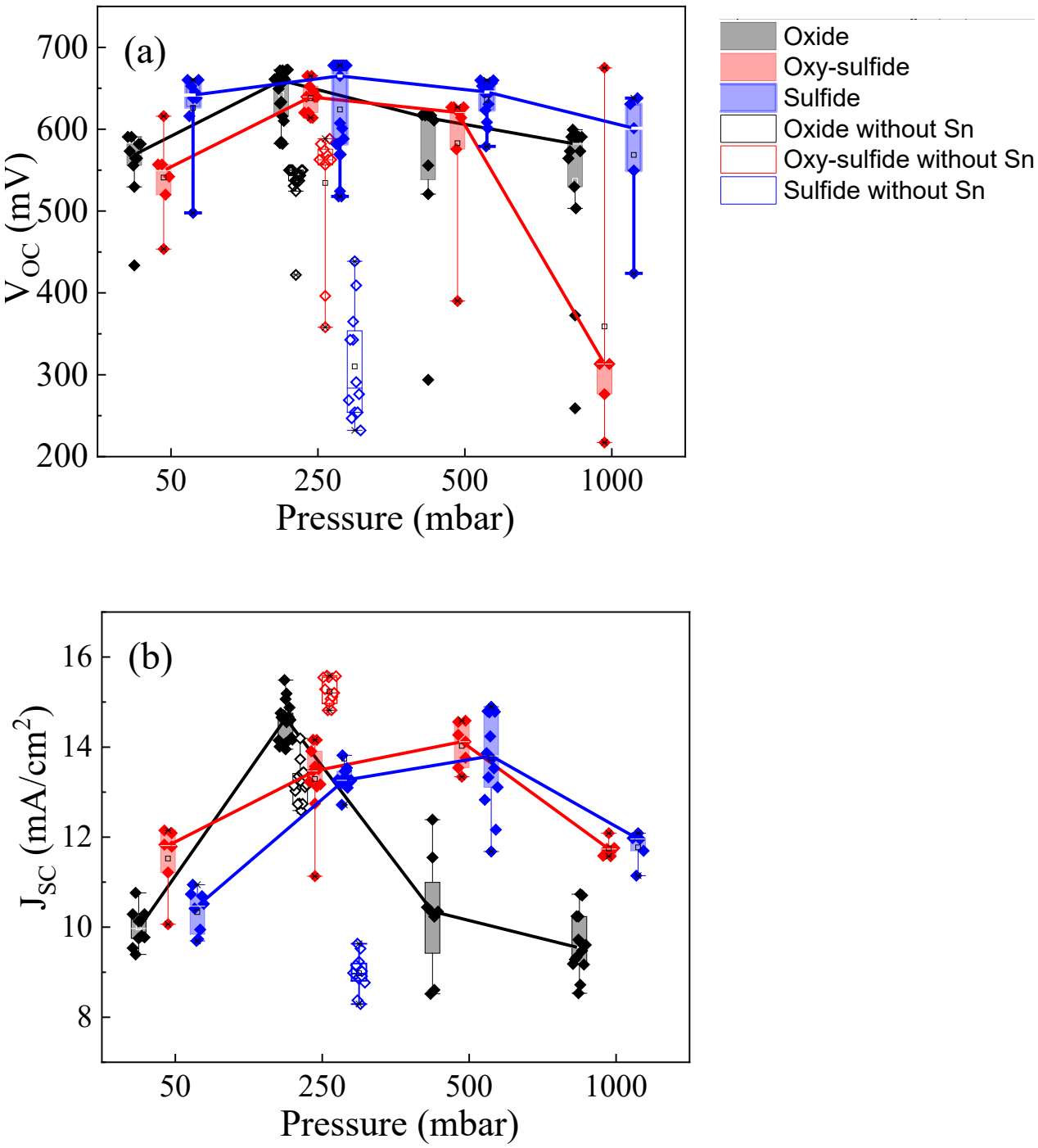
(a)
700
600
500
400
300
200
V_{OC} (mV)
50
250
500
1000
Pressure (mbar)
Oxide
Oxy-sulfide
Sulfide
Oxide without Sn
Oxy-sulfide without Sn
Sulfide without Sn
(b)
16
14
12
10
8
J_{SC} (mA/cm^2)
50
250
500
1000
Pressure (mbar)

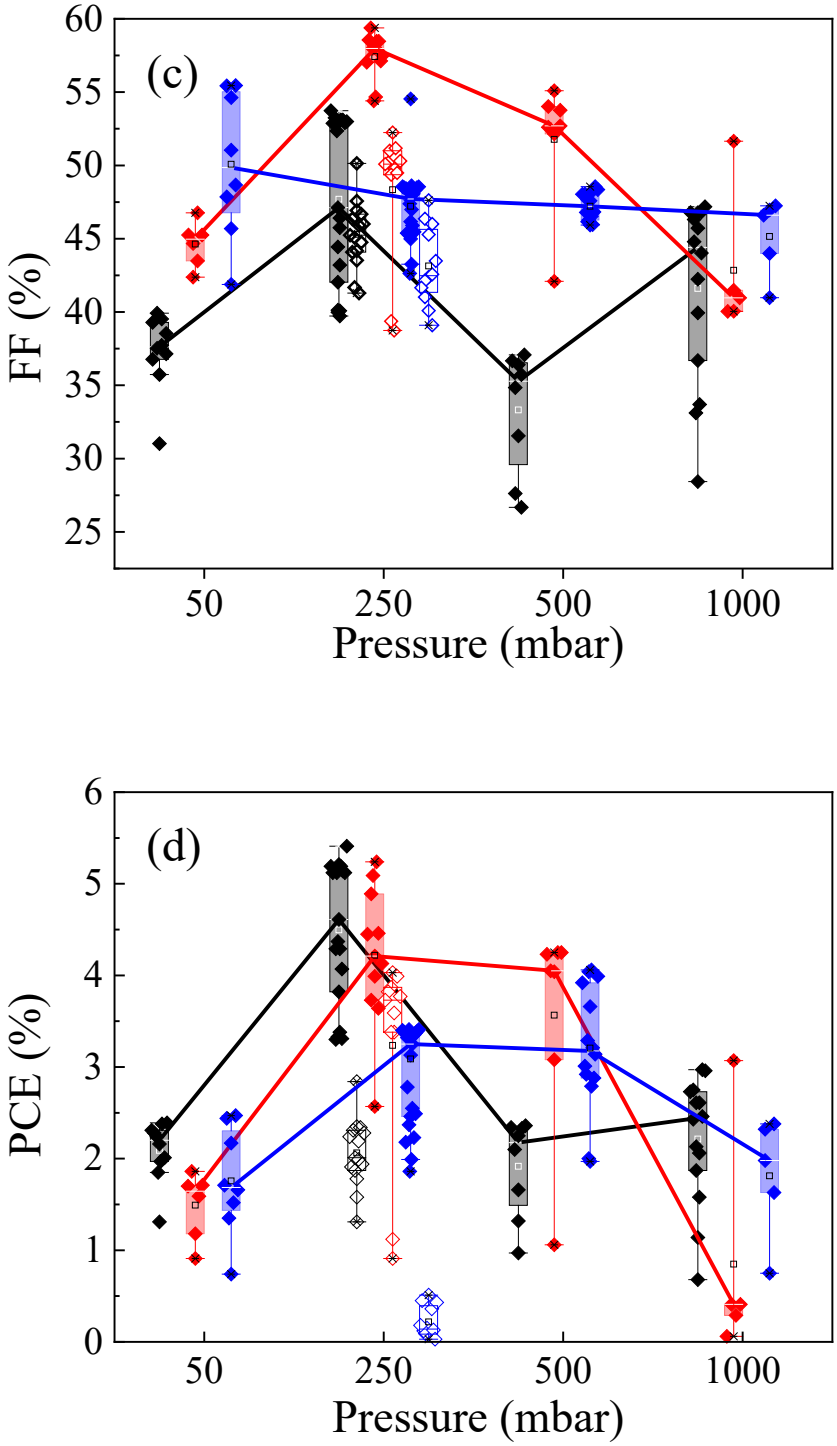

Fig. S8. Box plot of device parameters: open circuit voltage (V_{OC}) (a), short circuit current (J_{SC}) (b), fill factor (FF) (c) and power conversion efficiency (PCE) of oxide, oxy-sulfide and sulfide samples at different annealing pressure (d). Samples annealed without Sn powder are shown empty boxes. Data points are shown in diamond in corresponding color. Median values are connected with lines.

Table S1. O/(O+S) ratio before and after annealing on different precursors measured by EDX at 250 mbar annealing

Samples	**O/(O+S) ratio before annealing**	**O/(O+S) ratio after annealing**
Oxide	0.99	0.18
Oxy-sulfide	0.29	0.19
Sulfide	0.15	0.17